

Thermodynamics of Polymer Blends Organized by Balanced Block Copolymer Surfactants Studied by Mean-Field Theories and Scattering

Benedict J. Reynolds,^{†,‡} Megan L. Ruegg,[†] Nitash P. Balsara,^{*,†,§} Clayton J. Radke,^{*,†,‡} Timothy D. Shaffer,^{||} Min Y. Lin,^{||,#} Kenneth R. Shull,[⊥] and David J. Lohse^{||}

Department of Chemical Engineering, University of California, Berkeley, California 94720; Earth Science Division, Lawrence Berkeley National Laboratory, University of California, Berkeley, California 94720; Materials Sciences Division and Environmental Energy Technologies Division, Lawrence Berkeley National Laboratory, University of California, Berkeley, California 94720; ExxonMobil Research and Engineering, Annandale, New Jersey 08801; and Department of Materials Science and Engineering, Northwestern University, Evanston, Illinois 60208

Received February 2, 2004; Revised Manuscript Received June 11, 2004

ABSTRACT: Parameters determined from binary experiments were used to predict the behavior of multicomponent A/B/A–C polymer blends, where A is saturated polybutadiene with 90% 1,2-addition (sPB90), B is polyisobutylene (PIB), and C is also saturated polybutadiene but with 63% 1,2-addition (sPB63). The polymers were chosen such that the binary interactions (A/B, A/C, and B/C) are analogous to those in oil (A)/water (B)/nonionic surfactant (A–C) systems, where A/B and A/C are unfavorable interactions ($\chi > 0$) and B/C is a favorable interaction ($\chi < 0$). The Flory–Huggins interaction parameters (χ_{AB} , χ_{AC} , and χ_{BC}) and the statistical segment lengths (l_A , l_B , and l_C) were all determined experimentally by fitting the random phase approximation (RPA) to small-angle neutron scattering (SANS) data from the three binary homopolymer blends. These parameters were successfully used to predict the scattering from concentration fluctuations in a homogeneous A/B/A–C blend using multicomponent RPA. These same binary parameters were also used as the only inputs to self-consistent field theory (SCFT) calculations of ordered multicomponent polymer blends. The SCFT calculations enabled quantitative interpretation of the SANS profiles from microphase separated A/B/A–C blends. The phase separation temperatures predicted by theory for the blends were within the experimental error, and the theoretical domain spacings were within 10% of the experimental values.

Introduction

Most polymers are sparingly soluble in each other. This includes commodity polymers such as polyethylene, polypropylene, and polystyrene as well as more exotic polymers such as polythiophene, polyaniline, and polyferrocenylsilanes. Creating self-organized structures of one immiscible polymer in another is, therefore, of considerable technological interest. This requires the presence of suitable surfactants for stabilizing the interface between the immiscible polymers. The traditional approach for controlling the interface between two immiscible homopolymers labeled A and B is to use an A–B diblock (or graft) copolymer as a surfactant.^{1–29} It was generally believed that the affinity of the A block for the A homopolymer and that of the B block for the B homopolymer results in an accumulation of the copolymer at the interface. One then obtains a brush of A blocks emanating from the interface and penetrating into the A homopolymer phase and a complementary brush of B blocks penetrating into the B homopolymer phase. (Throughout this paper we will use “A block” to refer to the A chain that is part of the copolymer.) The copolymers in this system are thought to be analogous

to traditional surfactants with hydrophilic and oleophilic parts. However, there is no need to restrict our attention to A–B copolymers. For example, one may consider A–C block copolymers, particularly if the C block has attractive interactions with the B chains, or D–C block copolymers, wherein the D block and C block have attractive interactions with the A and B chains, respectively. Designing A–C and D–C surfactants requires a fundamental understanding of the phase behavior of multicomponent polymer blends with a multitude of attractive and repulsive interactions between the constituent chains. This paper is concerned with the thermodynamics of these kinds of polymer blends.

The phase behavior of homopolymer blends in the mean-field limit is usually described by the Flory–Huggins theory.^{30,31} In this theory the interactions between polymer chains are governed by the Flory–Huggins interaction parameter χ and the number of monomers per chain. Our understanding of the phase behavior of multicomponent blends containing block copolymers, such as those described above, rests on two theoretical frameworks: (1) the random phase approximation (RPA),^{32–34} which describes concentration fluctuations in single-phase systems, and (2) self-consistent field theory (SCFT),^{35–37} which describes the properties of micro- and macrophase-separated systems. The combination of Flory–Huggins theory, RPA, and SCFT provides a complementary set of theories for describing the thermodynamics of polymer mixtures, regardless of the number of components, the intricacy of molecular architecture (e.g., star block copolymers), and the complexity of phase behavior (e.g., coexisting ordered and disordered phases).

* Corresponding authors.

[†] Department of Chemical Engineering, UCB.

[‡] Earth Science Division, Lawrence Berkeley National Laboratory, UCB.

[§] Materials Sciences Division and Environmental Energy Technologies Division, Lawrence Berkeley National Laboratory, UCB.

^{||} ExxonMobil Research and Engineering.

[⊥] Northwestern University.

[#] Present address: NIST Center for Neutron Research, National Institute of Standards and Technology, Gaithersburg, MD 20899.

Mean-field theories have been used successfully to describe experimental data from traditional A/B polymer blends stabilized by A–B block copolymers.¹ The simplifying feature of A/B/A–B blends is that their phase behavior is governed by a single χ parameter because there are only two types of monomers.³⁸ Concentration fluctuations in single-phase A/B/A–B mixtures are in excellent agreement with predictions based on the RPA.^{10,11} Near phase boundaries, concentration fluctuations are announcements of impending phase transitions. Both macro- and microphase-separated systems are obtained, depending on the relative composition of the homopolymers and the block copolymer. The properties of the macrophase-separated systems are in good agreement with the Flory–Huggins theory while those of ordered microphase-separated systems are in good agreement with SCFT.^{39,40} An accurate description of the regime between ordered structures and macrophase-separated systems requires theories that account for the presence of fluctuations.^{17,26,41} Such theories are outside the scope of the present paper.

In recent work our group has demonstrated the efficacy of A–C copolymers for organizing blends of A/B homopolymers.^{42–44} The C block was chosen to have attractive interactions with one of the homopolymers (B), i.e., $\chi_{BC} < 0$. The other two χ parameters in the system, χ_{AB} and χ_{AC} , are positive, thus indicating repulsive interactions. We call these A–C copolymers “balanced surfactants”. The term balanced surfactants was originally used by Khalweit and co-workers to describe the properties of certain alkyl polyglycol ether molecules (often referred to as nonionic or $C_{12}E_6$ surfactants) in oil/water mixtures.⁴⁵ The term “balance” implies that the hydrophobic and hydrophilic interactions of these nonionic surfactant molecules are comparable in magnitude.^{45–51} Since hydrophobic generally implies oleophilic and hydrophilic implies oleophobic, the oleophilic and oleophobic interactions will also be comparable in magnitude. Similarly, our A–C copolymers are designed to balance the B-philic, B-phobic, A-philic, and A-phobic tendencies of the surfactant.

In the mean-field limit, the thermodynamics of A/B/A–C blends are, thus, characterized by three binary χ parameters: χ_{AB} , χ_{AC} , and χ_{BC} . The question that we address in this paper is the following: can the thermodynamic properties of complex polymer blends, wherein both attractive and repulsive interactions are present, such as our A/B/A–C blends, be predicted from interaction parameters and statistical segment lengths obtained from a priori binary experiments?

The answer to this question is obtained by a combination of theory and experiment. Small-angle neutron and light scattering experiments were conducted on a variety of mixtures of model polyolefins: component A was saturated polybutadiene with 90% 1,2-addition (sPB90), component B was polyisobutylene (PIB), and component C was saturated polybutadiene with 63% 1,2-addition (sPB63). (The prefix “s” stands for “saturated” and is replaced by “h” or “d” when we wish to specify whether the polymer is hydrogenated or deuterated.) We began by studying homogeneous binary sPB90/PIB, sPB63/PIB, and sPB63/sPB90 blends to obtain the binary interaction parameters and statistical segment lengths required to predict the phase behavior of the multicomponent systems. We then conducted scattering experiments on multicomponent blends of sPB90 and PIB homopolymers containing an sPB90–sPB63 block co-

polymer. The small-angle neutron scattering profiles of homogeneous sPB90/PIB/sPB90–sPB63 blends were compared with the predictions of the multicomponent random phase approximation. Increasing the molecular weights of the sPB90 and PIB homopolymers in the multicomponent studies leads to micro- and macrophase-separated systems, as expected. Theoretical predictions for the phase behavior of these multicomponent blends were obtained using self-consistent field theory. The binary experiments provided numerical values for all of the parameters needed for the multicomponent random phase approximation calculations as well as for the multicomponent self-consistent field theory calculations. This enabled a quantitative comparison of theory and experiment with no adjustable parameters.

Experimental Methods

Polybutadiene was synthesized via anionic polymerization in hexane at 0 °C using tetrahydrofuran (THF) as a polar additive to control the percent of 1,2- vs 1,4-addition. All reagents were purified under high vacuum. A trial-and-error method was employed to develop a calibration curve for the dependence of the percent 1,2- and 1,4-addition on initiator (*sec*-butyllithium) concentration and molar ratio of THF to initiator. A diblock copolymer of polybutadiene, with a different percent 1,2-addition for each of the blocks, was synthesized by sequential polymerization, in which the THF concentration in the reactor was adjusted after completing the polymerization of the first block. An aliquot of the first block (precursor) was isolated and terminated for characterization purposes, prior to the addition of the second block. The polymers were dried fully under vacuum at room temperature until they reached constant weight. They were then saturated (in solution in cyclohexane) using either hydrogen or deuterium gas in a Parr high-pressure reactor at 95 °C with a 5% palladium on barium sulfate catalyst. The hydrogenated polymers were again dried under vacuum at 150 °C for several days. In this paper we use the nomenclature sPB90 and sPB63 to describe saturated polybutadienes (with 90% and 63% 1,2-addition, respectively). The nomenclature hPB90/dPB90 and hPB63/dPB63 is used to distinguish between hydrogenated and deuterated polymers.

Polyisobutylene (PIB) was synthesized via cationic polymerization at –78 °C using a 60/40 ratio of hexane and methylene chloride as cosolvents. The cosolvents and monomer were purified under high vacuum. The initiator, 2-chloro-2,4,4-trimethylpentane (TMPCl), was synthesized by bubbling hydrogen chloride gas, produced through the addition of sulfuric acid to solid sodium chloride, continuously into a 2,4,4-trimethyl-1-pentene (TM1P) solution in methylene chloride with stirring for 3 days. Titanium(IV) chloride (TiCl_4) was used as the co-initiator, and dimethyl phthalate (DMP) was added as the proton trap. A solution of TiCl_4 in hexane was prepared in a separate side vessel and attached to the main reactor in a Vacuum Atmospheres glovebox filled with argon. TMPCl and DMP were added to the main reactor, and the entire apparatus was attached to a vacuum line. Polymerization was then carried out under full vacuum. The polymers were dried under vacuum at 150 °C for several days.

The molecular weights and architectures of the polymers were determined on a Waters 2690 gel permeation chromatography (GPC) system with a Viscotek triple detector. The three detectors (light scattering, viscometry, and refractometry) enabled the determination of the absolute number- and weight-averaged molecular weights (\overline{M}_n and \overline{M}_w) and the polydispersity index (PDI) of the homopolymers, the block copolymer precursor, and the block copolymer. The refractive indices of the polybutadiene/THF solutions were independent of the percent of 1,2 addition in the range of our experiments; this simplification enabled the characterization of the block copolymer. NMR spectroscopy was used to determine the percent 1,2- and 1,4-addition in all of the samples to an

Table 1. Polymer Properties^a

| polymer | M_w (kg/mol) | PDI | density at 23 °C (g/cm ³) | % 1,2 | n_D |
|--------------|-------------------|------|--|-------|-------|
| hPB90(10) | 10.1 | 1.01 | 0.8625 | 89 | NA |
| dPB90(10) | | 1.01 | 0.9020 | 89 | 2.54 |
| hPB63(10) | 9.9 | 1.02 | 0.8593 | 62 | NA |
| dPB63(10) | | 1.02 | 0.9125 | 62 | 3.44 |
| hPB90(35) | 34.9 | 1.02 | 0.8639 | 90 | NA |
| dPB90(35) | | 1.02 | 0.9037 | 90 | 2.56 |
| hPBPB(38–41) | 37.6–41.3 | 1.01 | 0.8633 | 63–92 | NA |
| dPBPB(38–41) | | 1.01 | 0.9098 | 63–92 | 2.99 |
| PIB(13) | 12.5 | 1.04 | 0.9134 | NA | NA |
| PIB(45) | 44.6 | 1.04 | 0.9140 | NA | NA |

^a h/dPB90(*x*) are saturated polybutadiene polymers, PIB(*x*) are polyisobutylene polymers, and h/dPBPB(*x*) are saturated polybutadiene diblock copolymers.

accuracy of $\pm 1\%$. An aliquot of the precursor of the diblock copolymer was analyzed by GPC and NMR. The extent of 1,2-addition of the second block was then determined from the known molecular weight and monomer volume of each block and the percent of 1,2-addition of the first block.

The characteristics of the polymers used in this study are summarized in Table 1. The composition labels for our samples are based on our targets. Samples wherein the % 1,2-addition deviated more than 2% from the targets were discarded.

The densities of the polymers at 23 ± 0.1 °C were measured using a density gradient column and are given in Table 1. The number of deuterium atoms per C₄ repeat unit, n_D , of each characterized polymer was obtained by comparing the densities of deuterated and hydrogenated polymer pairs obtained from the same polybutadiene precursor.

Binary and multicomponent blends of A, B, and A–C polymers were created by dissolving the components in hexane followed by precipitation in a 50/50 mixture of methanol and acetone. After precipitation was complete, the polymer was collected and placed on a 1 mm thick quartz disk inside a 1 mm thick spacer with an inner diameter of 14 mm. The sample was dried in a vacuum oven at 90 °C for 2 days to ensure complete removal of solvent. A second quartz disk was then placed on top of the polymer. The sample was pressed together at high temperature and annealed for 10 min at 90 °C. Unless otherwise stated, the samples studied in this paper were dried and annealed at 90 °C. To study the effect of thermal history on morphology, we repeated our experiments on samples that were dried and annealed at 150 °C. After cooling to room temperature, glue was placed around the edges of the sample in order to prevent leakage. The samples were stored at room temperature.

Small-angle neutron scattering (SANS) experiments were conducted on the NG1, NG3, and NG7 beamlines at the National Institute of Standards and Technology in Gaithersburg, MD. Using standard procedures, raw data were converted to absolute coherent scattering intensity, I , as a function of q ($q = 4\pi \sin(\theta/2)/\lambda$, θ is the scattering angle, λ is the wavelength of the incident beam), after corrections for detector sensitivity, background, empty cell, and incoherent scattering were made, using standard procedures.⁵² For the deuterated components, corrections for the nonuniformity of deuterium labeling were made.⁵³

Small-angle light scattering experiments were conducted with a 10 mW HeNe laser, with wavelength $\lambda_{\text{light}} = 633$ nm, directed through samples placed in a temperature-controlled heating unit. Scattered light was focused on a detector in the range of $4.33 \times 10^{-4} \text{ nm}^{-1} < q < 1.85 \times 10^{-3} \text{ nm}^{-1}$ using a beam stop and a focusing lens. (The definition of q given above holds for both light and neutron scattering.) Instrumental details are given in ref 54. The intensity was monitored as a function of time after the sample was heated in a stepwise manner from one predetermined temperature to another. The upper temperature limit of the light scattering sample holder was 250 °C.

Definitions

When using the RPA, it is convenient to describe our system as a mixture of “components”, where each component is a connected chain of identical monomers. Thus, our binary blends have two components while our A/B/A–C blends have four components. When using SCFT, it is convenient to describe our system as a mixture of “species”, where each species is a connected chain of (not necessarily identical) monomers. Thus, the A/B/A–C blends have three species. In both models we ignore the fact that the sPB90 and sPB63 chains are actually statistical copolymers. This is appropriate because both the RPA and SCFT in polymer mixtures are based on a coarse-grained view of polymer chains.⁵⁵

When discussing A/B/A–C ternary blends, the subscripts Ah and Bh refer to the A and B homopolymers, Ab and Cb refer to the A and C blocks of the copolymer, ACb refers to the entire block copolymer, and the subscripts A , B , and C refer to monomers of type A, B, or C. When discussing A/B, A/C, and B/C binary blends we use the subscripts A , B , and C to refer to the both the homopolymers and the monomer types (leaving out the h for notational simplicity).

The subscripts m and n are used to represent A , B , or C . In multicomponent RPA, summations over the subscripts j and k represent components Ah , Ab , and Cb (Bh is eliminated due to our assumption of incompressibility). In SCFT summations over the subscript i represent summations over Ah , Bh , and ACb . We use these three different conventions in order to simplify the equations that follow below.

We use a reference volume $v = 100 \text{ \AA}^3$, which is roughly the volume of a C₄ repeat unit of our components, as the basis for defining the following parameters: the Flory–Huggins interaction parameters χ_{mn} ($m, n = A, B, C$), the number of reference volume units per chain of each component (N_j), and the statistical segment lengths of the components (l_m), which describe the dependencies of the radius of gyration on N_j . Since the polymer density is temperature dependent, N_j is also temperature dependent.

Determination of Parameters from Binary Blend Small-Angle Neutron Scattering

The random phase approximation for the scattering intensity from a binary polymer blend is given by³²

$$I(q) = \frac{(b_A - b_B)^2}{v} \left(\frac{1}{N_A \phi_A P_A(q)} + \frac{1}{N_B \phi_B P_B(q)} - 2\chi_{AB} \right)^{-1} \quad (1)$$

where the Debye function, $P_m(q)$, is by definition

$$P_m(q) = \frac{2}{x_m} (\exp(-x_m) + x_m - 1) \quad (m = A, B, C) \quad (2)$$

b_m is the mean scattering length of each component (based upon a reference volume unit), N_m is the number of reference volume units in each component, ϕ_m is the spatially averaged volume fraction of each component, and $x_m = q^2 R_{g,m}^2 = q^2 N_m l_m^2 / 6$, where l_m is the statistical segment length of component m . (All parameters are based upon a reference volume of $v = 100 \text{ \AA}^3$.)

In Figure 1a–c we show the measured coherent SANS profiles, $I(q)$, from single-phase binary homopolymer blends at selected temperatures: (a) A/B [dPB90(10)/

Table 2. Binary Blend Compositions

| blend | component | | | ϕ_A | ϕ_B | ϕ_C |
|-------|-----------|---------|-----------|----------|----------|----------|
| | A | B | C | | | |
| A/B | dPB90(10) | PIB(45) | | 0.673 | 0.327 | |
| A/C | hPB90(10) | | dPB63(10) | 0.493 | | 0.507 |
| B/C | | PIB(13) | dPB63(10) | | 0.477 | 0.523 |

PIB(45)], (b) A/C [hPB90(10)/dPB63(10)], and (c) B/C [PIB(13)/dPB63(10)]. In each case the volume fractions of the polymers in the binary blends were the critical composition, as defined by the Flory–Huggins theory. The compositions of the binary blends are given in Table 2. The curves through the data in Figure 1a–c represent eq 1 with known values of ϕ_m and N_m (the monomer volume was calculated on the basis of the density of the polymer at 23 °C and its thermal expansion coefficient given in refs 56 and 57) and χ_{mn} and l_m as adjustable parameters. Our protocol for obtaining χ_{mn} and l_m is slightly different from that used in previous studies.^{10,11} The SANS profiles from all three binary blends were measured at approximately 30, 90, and 170 °C. The values of χ_{mn} and l_m were fit simultaneously to the three sets of data at these temperatures, thereby ensuring that the statistical segment lengths for each polymer obtained from different blends were identical. For example, the values of l_A obtained from A/B and A/C blends at 30 °C were constrained to be the same. The RPA is based on the assumption that the chain conformations in the blends are not affected by the presence of other chains. Our fitting procedure is consistent with this assumption. The dashed curves in Figure 1a–c through the data at 30, 90, and 170 °C are the results of the above-mentioned fitting procedure. The dashed curves are barely visible behind the solid curves, which will be described shortly. It is evident that all of the features of the scattering profiles are captured quantitatively by our fitting procedure. This enables the determination of the temperature dependence of l_A , l_B , and l_C shown in Figure 2. In Figure 2, we have plotted the parameter $l_{mon,m} = l_m \sqrt{v_{mon,m}/v}$, where $v_{mon,m}$ is the monomer volume based on a C_4 repeat unit. This parameter ($l_{mon,m}$) is the statistical segment length based upon the C_4 repeat unit volume. The two statistical segment lengths are related as follows: $N_m l_m^2 = N_{mon,m} l_{mon,m}^2$ ($N_{mon,m}$ is the number of C_4 repeat units per chain.)

It is clear from Figure 2 that $l_{mon,m}$ are temperature-independent, indicating that the radius of gyration of our chains is temperature-independent. The dashed lines in Figure 2 indicate the average values of $l_{mon,m}$. Taking $l_{mon,A} = 0.51$ nm, $l_{mon,B} = 0.61$ nm, and $l_{mon,C} = 0.78$ nm (the average values of the statistical segment lengths shown in Figure 2) is an excellent approximation across the temperature range studied. We refit all of the binary blend data from A/B, A/C, and B/C blends with fixed values of $l_{mon,A}$, $l_{mon,B}$, and $l_{mon,C}$. χ_{mn} was the only adjustable parameter. The solid curves in Figure 1a–c are the results of this fitting protocol. At 30, 90, and 170 °C the theoretical curves obtained by fitting χ_{mn} and l_m (dashed curves) and those obtained by fitting χ_{mn} only (solid curves) are almost indistinguishable. The statistical segment lengths of our components are in reasonable agreement with previous measurements where values $l_{mon,A} = 0.57$ nm, $l_{mon,B} = 0.57$ nm, and $l_{mon,C} = 0.67$ nm were obtained at 25 °C, using data from only one polymer blend.⁵⁸ In contrast our values were obtained by enforcing consistency between data obtained

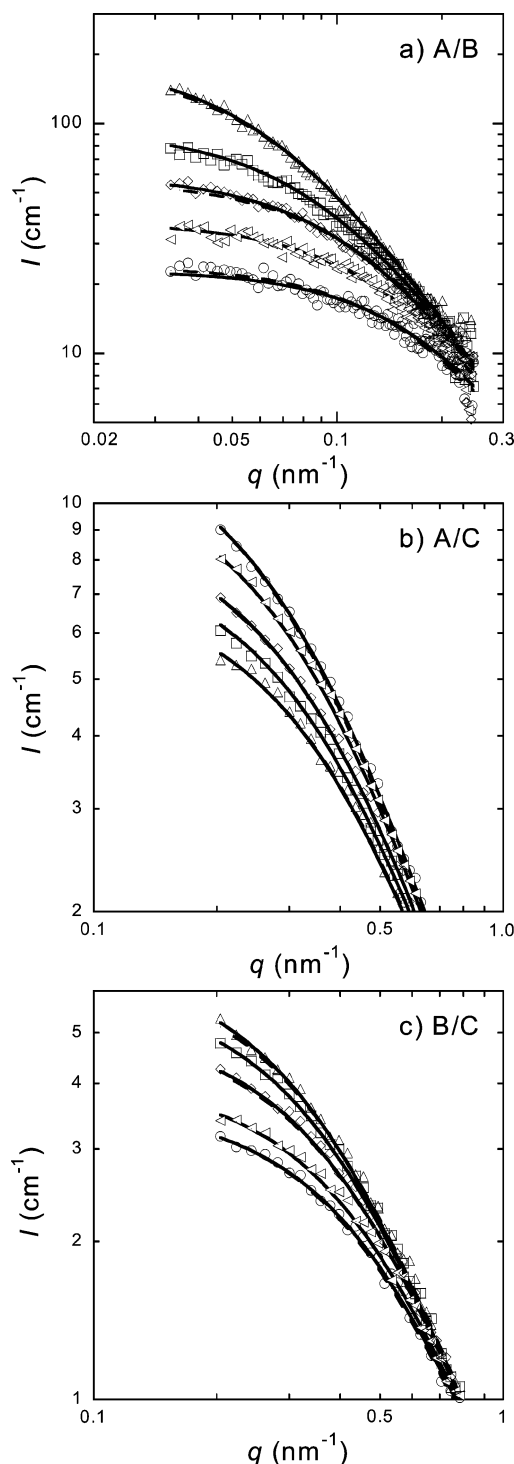


Figure 1. SANS from binary blends of (a) A/B homopolymers [dPB90(10)/PIB(45)], (b) A/C homopolymers [hPB90(10)/dPB63(10)], and (c) B/C homopolymers [PIB(13)/dPB63(10)] at selected temperatures. The dashed lines are the random phase approximation fit to the data with χ_{mn} and l_m as adjustable parameters. The solid lines are the random phase approximation fit to the data with χ_{mn} as an adjustable parameter but with $l_{mon,m}$ constrained to a temperature-independent value. (a) data markers: 30 (○), 60 (tilted △), 90 (◇), 119 (□), and 169 °C (△). (b, c) data markers: 29 (○), 50 (tilted △), 92 (◇), 134 (□), and 175 °C (△).

from two independent and chemically distinct polymer blends.

The temperature dependencies of the χ parameters obtained from the second fitting procedure described above (solid curves in Figure 1) are given in Figure 3.

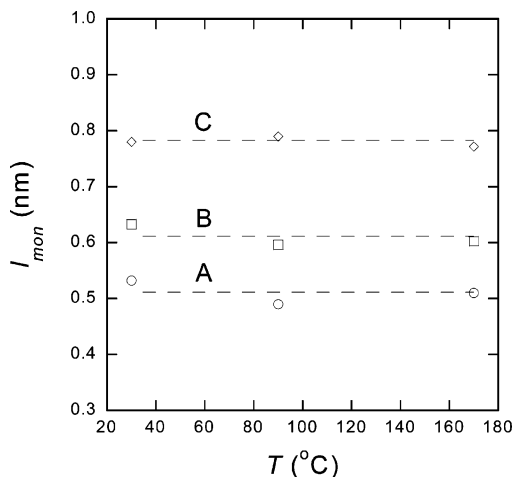


Figure 2. Statistical segment lengths [$l_{mon,A}$ (○), $l_{mon,B}$ (□), $l_{mon,C}$ (◇)] obtained from fitting the random phase approximation to the binary homopolymer blend scattering profiles at 30, 90, and 170 °C. Dashed lines indicate average $l_{mon,m}$ values.

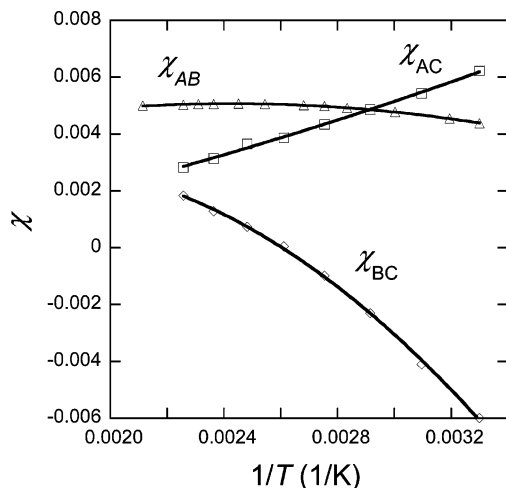


Figure 3. χ parameters obtained for the three binary blends: A/B (Δ), A/C (\square), and B/C (\diamond) from RPA fits.

These are the χ parameters that will be used in the multicomponent RPA and SCFT calculations. The curves through the data in Figure 3 represent least-squares fits of the equation $\chi = A + B/T + C/T^2$. The temperature dependencies of the interaction parameters in our system are, thus, given by the following equations:

$$\chi_{AB} = -0.000443 + 4.52 \frac{1}{T} - 927 \frac{1}{T^2} \quad (3)$$

$$\chi_{AC} = -0.00147 + 1.32 \frac{1}{T} + 300 \frac{1}{T^2} \quad (4)$$

$$\chi_{BC} = -0.00527 + 10.3 \frac{1}{T} - 3168 \frac{1}{T^2} \quad (5)$$

Our expression for χ_{BC} is similar to that given in ref 59. Our expression for χ_{AC} is consistent with predictions based on the solubility parameters given in ref 60. To our knowledge, χ_{AB} has not been previously measured. The χ values reported in eqs 4 and 5 are within 10–20% of previously measured values. Linear fitting parameters⁶¹ are normally used to describe the temperature dependence of χ . We used a quadratic fit in order to increase the accuracy of the binary parameters

Table 3. Multicomponent Blend Compositions

| blend | component | | | ϕ_A | ϕ_B | ϕ_{AC} |
|-------|-----------|---------|--------------|----------|----------|-------------|
| | A | B | A–C | | | |
| B40 | dPB90(35) | PIB(45) | hPBPB(38–41) | 0.316 | 0.284 | 0.400 |
| B40-2 | dPB90(35) | PIB(45) | hPBPB(38–41) | 0.316 | 0.284 | 0.400 |
| B40b | hPB90(35) | PIB(45) | dPBPB(38–41) | 0.316 | 0.284 | 0.400 |
| B50 | dPB90(35) | PIB(45) | hPBPB(38–41) | 0.264 | 0.237 | 0.500 |
| B50-2 | dPB90(35) | PIB(45) | hPBPB(38–41) | 0.264 | 0.237 | 0.500 |
| B50b | hPB90(35) | PIB(45) | dPBPB(38–41) | 0.264 | 0.237 | 0.500 |
| BH20 | dPB90(10) | PIB(13) | hPBPB(38–41) | 0.400 | 0.400 | 0.200 |

used as inputs for multicomponent RPA and SCFT. It is evident from Figure 3 that the three binary interactions are qualitatively different from each other. χ_{AB} is a very weak function of temperature, varying between 0.0044 and 0.0051 when the temperature is changed from 30 to 200 °C. Flory–Huggins theory can be used to calculate χ_c , the value of χ at the critical point (eq 6). In a symmetric blend, $\chi_{AB}N = 2$ ($N = N_A = N_B$). In an asymmetric blend, $\chi_{AB}N_{ave} = 2$, where N_{ave} is defined by

$$\chi_c = 2 \left[\frac{1}{2(N_A)^{1/2}} + \frac{1}{2(N_B)^{1/2}} \right]^2 = \frac{2}{N_{ave}} \quad (6)$$

The product $\chi_{AB}N_{ave}$ for the A/B blend changes by about 10% in our temperature window (from 1.6 to 2.0). We made several critical A/B blends with varying molecular weights of the components and found that the blends that were homogeneous at room temperature remained homogeneous at all temperatures, whereas those that were phase separated at room temperature remained phase separated at all temperatures. Identifying an A/B blend that enabled determination of the χ parameter, thus, involved considerable trial-and-error. Note that all the temperature dependence of the SANS profiles in Figure 1a, seen despite the relative temperature insensitivity of χ_{AB} (Figure 3), is due mainly to the proximity of χ to χ_c . The value of χ_c for this A/B blend is 0.0051, as determined from eq 6.

Since the incompatibility between the two homopolymers that we wish to organize is a weak function of temperature, the temperature dependence of the thermodynamic properties of our blends is mostly caused by the temperature dependence of the interactions between the A–C surfactant and the homopolymers, i.e., the temperature dependencies of χ_{BC} and χ_{AC} . As shown in Figure 3, χ_{BC} is negative over much of our temperature window and it increases with increasing temperature. On the other hand, χ_{AC} is positive over the entire temperature window, and it decreases with increasing temperature (Figure 3). These opposite dependencies of χ_{BC} and χ_{AC} on temperature are, in our view, an essential feature of balanced surfactants.

Scattering from A/B/A–C Blends

Ternary A/B/A–C blends were prepared with the ratio ϕ_{A1}/ϕ_{B1} set by the critical volume fraction for the binary A/B blends based upon Flory–Huggins theory. In all cases the surfactant was either the hPBPB(38–41) or the dPBPB(38–41) block copolymer. Compositions of the blends are shown in Table 3. The surfactant volume fraction serves as a convenient way of characterizing blend composition. In Figure 4 we present the SANS profile obtained from blend BH20, containing dPB90(10)/PIB(13)/hPBPB(38–41) with 20% surfactant, at 30 °C. This blend was single phase at all accessible tem-

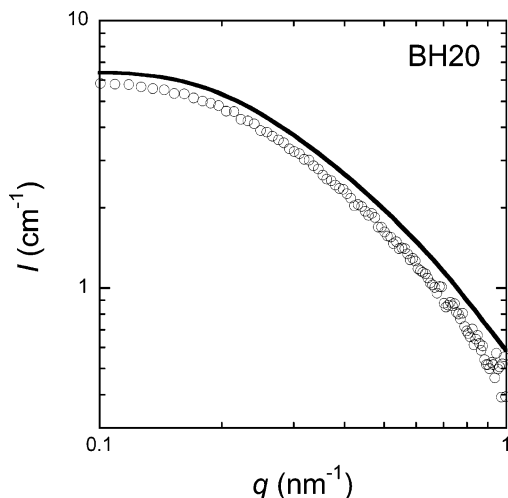


Figure 4. SANS profile obtained from blend BH20 at 30 °C. Solid line indicates multicomponent RPA predictions with no adjustable parameters (see Appendix A).

peratures. This is not surprising because for this blend the product $\chi_{AB}N_{ave}$ is 0.95–1.21 across our temperature range which is significantly smaller than 2. The solid curve in Figure 4 is the theoretically predicted SANS profile for the dPB90(10)/PIB(13)/hPBPB(38–41) blend using multicomponent RPA. The equations used to obtain the curve are given in Appendix A. All of the parameters needed for the theoretical calculations were obtained from the binary experiments. Previous studies have shown that the effect of deuterium labeling is small compared to the magnitudes of the χ parameters in eqs 3–5.^{60,62–64} The χ parameters used in the multicomponent RPA and SCFT calculations are those given in eqs 3–5 and have not been adjusted to account for deuterium labeling. The nearly quantitative agreement between theory and experiment seen in Figure 4 is remarkable. The deviations between theory and experiment are less than 1 cm⁻¹, at all accessible q . Note that the theoretical curves are based entirely on binary blend data and that all aspects of the interactions between the hPBPB(38–41) block copolymer and the other species in our system are derived from these binary results. The temperature dependence of the theoretical and experimental scattering profiles of blend BH20 was unremarkable. Thus, for brevity we do not show the data obtained at other temperatures.

We now discuss SANS profiles of blends of sPB90-(35)/PIB(45)/sPBPB(38–41). Note that the molecular weights of the homopolymers in these blends are significantly larger than those in blend BH20. The product $\chi_{AB}N_{ave}$ for homopolymers A and B used here is 3.34–4.25 across the temperature range, indicating strong repulsive interactions between them. We thus expect blends containing these polymers to be either micro- or macrophase-separated. For critical polymer blends containing symmetric block copolymers, lamellae and microemulsions are the two kinds of microphase-separated structures expected.³ The lamellar phase has long-range order, and reproducible scattering profiles are only obtained if the sample is perfectly aligned or if the sample is a perfect powder. In soft polymeric systems, it is relatively easy to obtain partially aligned lamellar phases when the material is loaded into the sample cell.⁶⁵ Thus, the detailed features of the scattering profiles obtained from different lamellar samples are often azimuthally inhomogeneous and dependent on

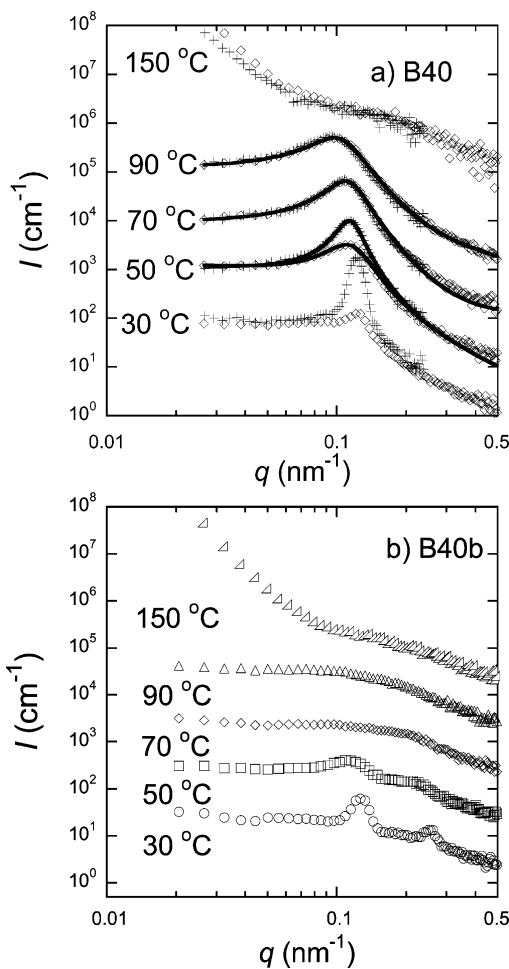


Figure 5. (a) SANS profiles obtained from blends B40 and B40-2 at selected temperatures (for B40 the temperatures were 30, 50, 70, 90, and 150 °C; for B40-2 the temperatures were 29, 50, 71, 92, and 154 °C). The open diamonds are the data taken from sample B40, and the plus signs are the data taken from sample B40-2. For 30 and 50 °C, the data taken from B40-2 has a higher intensity than the data taken from B40. The solid lines are the Teubner–Strey scattering profile fit to the data. To delineate the data, each data set has been multiplied by the following factors: 1 (30 °C), 10 (50 °C), 10² (70 °C), 10³ (90 °C), 10⁵ (150 °C). (b) SANS profiles obtained from blend B40b at selected temperatures: 30 °C (○), 50 °C (data set multiplied by 10) (□), 70 °C (data set multiplied by 10²) (◇), 90 °C (data set multiplied by 10³) (△), and 150 °C (data set multiplied by 10⁴) (tilted △).

loading conditions, thermal history, etc. Microemulsions, on the other hand, do not possess long-range order, and scattering profiles obtained from these systems are azimuthally homogeneous and independent of processing history. We use these facts to analyze SANS data from blends labeled B40 and B50, which contain 40% and 50% block copolymer, respectively. The deuterated component in these blends is the dPB90 homopolymer. In addition, blends labeled B40-2 and B50-2 were prepared and were identical to blends B40 and B50, respectively, except that they were annealed at 150 °C rather than 90 °C (see Experimental Methods section). We also studied blends with compositions that were identical to B40 and B50, except for the fact that the deuterated component was the block copolymer. We call these blends B40b and B50b.

Small-angle neutron scattering profiles from B40 and B40-2 at selected temperatures are shown in Figure 5a. At temperatures between 30 and 90 °C, the SANS data

Table 4. Teubner–Strey Scattering Profile Fit to B40 and B50 Blends

| blend | a (cm) | b (cm–nm ²) | c (cm–nm ⁴) | d (nm) | ξ (nm) |
|---------------|----------|---------------------------|---------------------------|----------|------------|
| B40 (50 °C) | 0.0172 | –2.27 | 93.30 | 55.39 | 37.93 |
| B40 (70 °C) | 0.0106 | –1.53 | 64.25 | 56.52 | 45.51 |
| B40 (90 °C) | 0.0083 | –1.31 | 68.91 | 62.10 | 37.51 |
| B40-2 (50 °C) | 0.0150 | –2.18 | 85.16 | 55.02 | 66.45 |
| B40-2 (71 °C) | 0.0117 | –1.76 | 75.82 | 57.32 | 49.65 |
| B40-2 (92 °C) | 0.0082 | –1.43 | 80.24 | 64.46 | 40.40 |
| B50 (50 °C) | 0.0349 | –3.54 | 98.23 | 46.29 | 48.83 |
| B50 (70 °C) | 0.0330 | –3.20 | 94.34 | 47.06 | 33.61 |
| B50 (90 °C) | 0.0299 | –2.69 | 93.59 | 49.50 | 23.87 |
| B50-2 (50 °C) | 0.0379 | –3.95 | 11.15 | 46.73 | 52.66 |
| B50-2 (71 °C) | 0.0364 | –3.64 | 10.82 | 47.38 | 36.19 |
| B50-2 (92 °C) | 0.0292 | –2.75 | 99.06 | 50.46 | 24.61 |

for both B40 and B40-2 show a peak at q values between 0.10 and 0.12 nm^{–1}, indicating the presence of periodic structures. The intensities of the peaks at 30 and 50 °C for B40 and B40-2 differ substantially. In addition, the two-dimensional scattering profile from B40 was azimuthally inhomogeneous while that from B40-2 was homogeneous. These are characteristics of periodic phases with long-range order (e.g., lamellae). In contrast, at 70 and 90 °C the scattering profiles for B40 and B40-2 are identical and azimuthally homogeneous. These are characteristics of disordered phases (e.g., a microemulsion).

The scattering from microemulsions in the vicinity of the primary maximum is often described by the Teubner–Strey (TS) equation:⁵¹

$$I(q) = \frac{1}{a + bq^2 + cq^4} + I_{bgd}(q) \quad (7)$$

where a , b , and c are fitting parameters and we use $I_{bgd}(q)$ to account for the fact the TS equation was developed for oil/water microemulsions and thus does not account for scattering contributions due to the connectivity of polymer chains. $I_{bgd}(q)$ is assumed to be of the form $I_{bgd}(q) = (eq^2 + f)^{-1}$, where e and f are fitting constants.⁶⁶ The curves in Figure 5a are the least-squares fits of eq 7 through the data with a , b , c , e , and f as adjustable constants. The values of the constants are given in Table 4 for all data sets. We take agreement between the TS equation and our data to be indicative of the presence of a microemulsion.⁵¹ On the basis of this, the agreement between the scattering profiles obtained from B40 and B40-2, and their azimuthal homogeneity, we conclude that sample B40 is a microemulsion at 70 and 90 °C. It is perhaps appropriate to add here that our attempts to fit the 30 °C data of B40 to the TS equation were unsuccessful. We do not believe that this scattering profile can be fit with the TS equation without using an unphysical background term.

The domain spacing (d) and correlation length (ξ) can be calculated from the TS fit parameters a , b , and c by

$$\xi = \left[\frac{1}{2} \frac{a}{c} \right]^{1/2} + \frac{1}{4} \frac{b}{c} \quad (8)$$

$$d = 2\pi \left[\frac{1}{2} \frac{a}{c} \right]^{1/2} - \frac{1}{4} \frac{b}{c} \quad (9)$$

The values of d and ξ for our blends are given in Table 4. The TS equation applies equally well to both droplet and bicontinuous microemulsions. Thus, we are not sure if the d values obtained here correspond to the distance

between adjacent droplets or the characteristic length of bicontinuous phases.

To understand the nature of the phase at 30 °C in blends B40 and B40-2, we also examined blend B40b with neutron scattering. The scattering data from B40b are shown in Figure 5b. At 30 °C the presence of two peaks, at $q_1 = 0.127$ nm^{–1} and $q_2 = 0.254$ nm^{–1}, is observed.⁶⁷ The fact that $q_2 = 2q_1$ indicates the presence of a lamellar phase. This is consistent with our analysis of the data from B40 and B40-2 at 30 °C. We thus conclude that sample B40 is lamellar at 30 °C.

The state of B40 at 50 °C is not clear. The two scattering peaks at $q_1 = 0.113$ nm^{–1} and $q_2 = 0.218$ nm^{–1} ($q_2 = 2q_1$ within experimental error) observed from B40b (Figure 5b) and our observations of the scattering profiles from B40 and B40-2 (Figure 5a) suggest that we have a lamellar phase. However, the B40 and B40-2 data are consistent with the Teubner–Strey equation, which suggests that the blend is a microemulsion. On the basis of the criteria that we have established above, we thus cannot uniquely determine the structure of B40 at 50 °C. The Gibbs phase rule requires a region of coexistence between two multicomponent one-phase systems. Perhaps our difficulties in determining the structure of B40 at 50 °C are due to the coexistence of lamellae and microemulsions.

The data obtained from B40b at 70 and 90 °C shown in Figure 5b do not show pronounced features and thus do not affect our conclusion based on B40 and B40-2 that the sample is a microemulsion at these temperatures. We will discuss these profiles in more detail after the SCFT calculations are described.

While a relatively low scattering intensity is observed at low q at temperatures < 112 °C for blends B40, B40-2, and B40b (Figure 5a,b), a significantly larger scattering intensity is observed at low q at temperatures ≥ 112 °C. For example, $I(q = 0.03$ nm^{–1}) of B40 at 30 °C is 75 cm^{–1} (Figure 5a) and that of B40b at 30 °C is about 25 cm^{–1} (Figure 5b). However, $I(q = 0.03$ nm^{–1}) of B40 at 150 °C is about 700 cm^{–1} (Figure 5a) and that of B40b at 150 °C is about 1400 cm^{–1} (Figure 5b). This is a standard signature of macrophase separation. We have not shown the scattering profiles at 112 °C as they were qualitatively similar to that at 150 °C. We thus conclude that our system exhibits macrophase separation in the vicinity of 112 °C.⁶⁸ The large low- q scattering intensity from the B40b sample (Figure 5b) indicates that the block copolymer preferentially segregates into one of the macrophases. Around 112 °C, χ_{BC} is approximately equal to zero (see Figure 3). Since χ_{AB} is greater than χ_{AC} , we expect the diblock copolymer to be located in the A phase at this temperature.

We have now identified three kinds of phases in B40 and B40b: a lamellar phase at 30 °C, a microemulsion at temperatures between 70 and 90 °C, and a macrophase-separated state above 112 °C.

The reason for the difference in scattering profiles obtained from the B40 and B40-2 lamellar phases should now be clear. B40 was annealed and pressed when it was a microemulsion, while B40-2 was annealed and pressed in the phase-separated state. Given these differences, the quantitative agreement between B40 and B40-2 (Figure 5a) at 70 and 90 °C is noteworthy.

Small-angle light scattering was also used to study the phase behavior of blend B40. Macrophase separation is indicated by high light scattering intensities.⁶⁸ An ordered structure on the submicron scale and a disor-

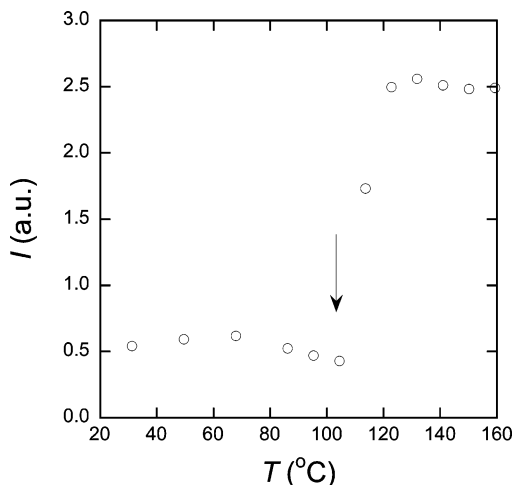


Figure 6. SALS data obtained from blend B40-2. The arrow represents the one-to-two-phase transition temperature.

Table 5. Comparison of One-to-Two Phase Transition Temperatures for Blends B40-2 and B50-2

| blend | T_{trans} based on SANS (°C) | T_{trans} based on SALS (°C) |
|-------|---------------------------------------|---------------------------------------|
| B40-2 | 103 ± 11 | 104 ± 5 |
| B50-2 | 103 ± 11 | 113 ± 5 |

dered sample exhibit a negligible light scattering intensity. Figure 6 shows the small-angle light scattering data obtained from blend B40. At low temperatures (below 104 °C), we observe a small light scattering intensity, which indicates a one-phase state. At high temperatures (above 104 °C) we observe an increasingly larger light scattering intensity, which indicates macrophase separation (a two-phase state). The macrophase separation temperature determined from light scattering is indicated by the arrow in Figure 6. This temperature is in excellent agreement with the conclusions based on SANS data (Figure 5a). Comparison of the one-to-two-phase transition temperatures as obtained from SANS and SALS for blend B40-2 is given in Table 5.

In Figure 7a,b we show the SANS profiles obtained from (a) B50 and (b) B50b at selected temperatures. SANS measurements were also made from the B50-2 sample; however, these data are identical to those obtained from B50 and will therefore not be discussed. We find that the phase behavior of blends B50 and B40 are very similar (compare Figures 5a and 7a). Accordingly, we find a lamellar phase at 30 °C, a microemulsion phase at temperatures between 70 and 90 °C, and a macrophase-separated state at high temperatures above 112 °C. For reasons that are not clear, it appears that we obtain random grain orientations in the lamellar phase, regardless of whether the samples were annealed at 90 or 150 °C. Light scattering data obtained from B50-2 (not included for brevity) confirm the onset of macrophase separation at about 112 °C.

A comparison of the one-to-two-phase transition temperatures as obtained from SANS and SALS for blend B50-2 is given in Table 5.

Mean-Field Theory for A/B/A–C Mixtures

The SANS data from our A/B/A–C blends indicate the existence of three kinds of systems: lamellae, microemulsions, and phase-separated systems. We use Flory–Huggins theory and self-consistent field theory to develop a simple mean-field picture that can predict the conditions (temperature and composition) under which

lamellae and phase-separated systems occur and the length scale of the periodicity, if periodic phases are obtained. Because of the one-dimensional nature of our calculations and because self-consistent field theory neglects the effect of fluctuations, we are unable to model microemulsions.

We begin with the Flory–Huggins expression for the Helmholtz free energy per unit volume, f , of a structureless A/B/A–C mixture.

$$\frac{fv}{kT} = \sum_i \frac{\phi_i}{N_i} \ln \phi_i + \sum_{m,n} \chi_{mn} \phi_m \phi_n - \sum_{i,m,n} \frac{\chi_{imn} \phi_{i,m} \phi_{i,n}}{\phi_i} \quad (10)$$

where v is the reference volume, $i = (Ah, Bh, ACb)$, ϕ_{Ah} , ϕ_{Bh} , and ϕ_{ACb} are the average volume fractions of the A homopolymer, B homopolymer, and A–C diblock copolymer, respectively, and N_{Ah} , N_{Bh} , and N_{ACb} are the number of reference volume units in the three species. The subscripts m and n represent the set (A, B, C) where ϕ_A , ϕ_B , and ϕ_C are the average volume fractions of monomers of type A, B, and C, and χ_{AB} , χ_{AC} , and χ_{CB} are the three interaction parameters. The notation $\phi_{i,m}$ will be used to represent the volume fraction of monomer of type m from species of type i , where $m = (A, B, C)$ and $i = (Ah, Bh, ACb)$, i.e., $\phi_A = \phi_{Ah,A} + \phi_{Bh,A} + \phi_{ACb,A} = \phi_{Ah} + \phi_{Ab}$. The reference state, implicit in this expression for the free energy, is that of each species forming a pure structureless phase.

Periodic structures are described using self-consistent field theory (Appendix B).^{35–37} In these phases the volume fractions of the components, $\phi_{i,m}$, are periodic functions of position. We use $\phi_{i,m}(z)$ to describe these functions, while the term $\phi_{i,m}$ refers to the average value of $\phi_{i,m}(z)$. The parameter z is a Cartesian one-dimensional coordinate made dimensionless using $v^{1/3}$. By assuming that our concentration profiles vary only in one linear dimension, we restrict ourselves to lamellar periodic structures. Self-consistent field theory substitutes interactions between the polymers for equivalent external fields. Given these external fields, the volume fraction profiles, $\phi_{i,m}(z)$, are found that minimize the free energy. Self-consistency then requires that the external fields, produced by the volume fraction profiles, must be consistent with the external fields originally proposed. In this work SCFT is used to calculate the volume fraction profiles, $\phi_{i,m}(z)$, and free energy densities, f , of ordered structures and to find the interfacial tension between two disordered phases. A detailed description of the method is given in refs 35–37. The procedure employed in this work is described in Appendix B.

Comparison of Theory and Experiment

Figure 8 shows a typical theoretical composition profile calculated using the SCFT procedure described in Appendix B. The volume fractions are plotted against $zv^{1/3}$ for blend B40 at 30 °C with a lamellar spacing of 50 nm. The free energy densities, f , can be calculated for a number of different lamellar spacings, and the dependence of f on lamellar spacing, d , for B40 at 30 °C, is shown in Figure 9. The location of the minimum is found by fitting a parabola to the lowest points. A clear minimum is seen in Figure 9 at a lamellar spacing of 51 nm. It is thus clear that the results for the 50 nm lamellar spacing chosen for B40 in Figure 8 give the characteristics of the equilibrium lamellar phase at 30 °C.

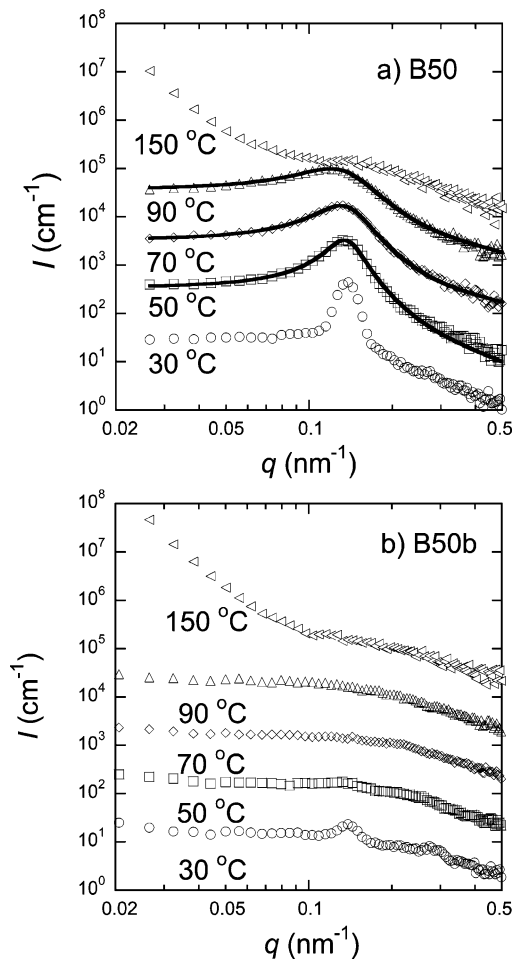


Figure 7. SANS profiles obtained from (a) blend B50 and (b) blend B50b at selected temperatures: 30 °C (○), 50 °C (□), 70 °C (◇), 90 °C (△), and 150 °C (tilted △). The solid lines are the Teubner–Strey scattering profile fit to the data. To delineate the data, each data set in both (a) and (b) has been multiplied by the following factors: 1 (30 °C), 10 (50 °C), 10² (70 °C), 10³ (90 °C), 10⁴ (150 °C).

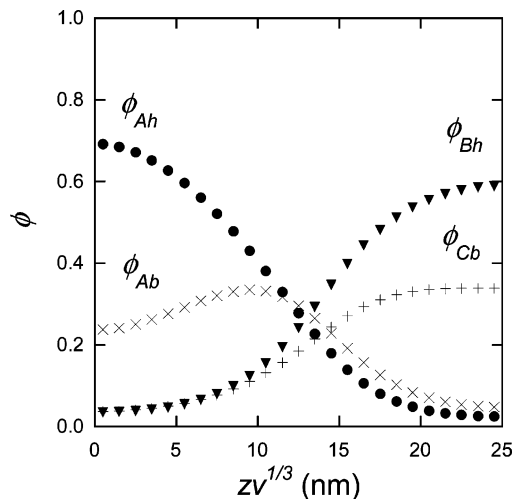


Figure 8. Volume fraction profiles of the components, calculated using SCFT for blend B40 at 30 °C with a box size of 25 nm. The components are the sPB90 homopolymer (●), the PIB homopolymer (▼), the sPB90 block of the diblock copolymer (×), and the sPB63 block of the diblock copolymer (+).

The composition profiles shown in Figure 8 are instructive as they show details regarding the distribution of various components in the periodic structure. The

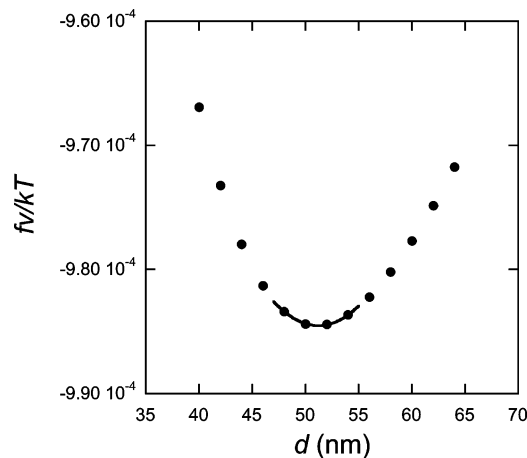


Figure 9. Free energy densities of lamellar structures of different spacings for blend B40 at 30 °C with a parabola fit to the four minimum points.

composition profiles of the A and B homopolymers are unremarkable and are as expected on the basis of the value of χN_{ave} at 30 °C. An interesting asymmetry is seen in the arrangement of the A and C blocks of the block copolymer. The A block accumulates near the A/B interface (note the maximum in ϕ_{Ab} near the interface) while the C block penetrates deeper into the B-rich phase (the maximum in ϕ_{Cb} is in the center of the B-rich region).

The primary scattering peak from sample B40 at a given temperature is significantly stronger than that from B40b at the same temperature (Figure 5a,b). On this basis, one might expect to see stronger higher order peaks in B40 than in B40b. This is clearly not the case. On the contrary, we were unable to find any evidence of second-order lamellar peaks in B40.

To understand the origin of this puzzling observation, neutron scattering length density profiles, $\rho(zV^{1/3})$, were derived from the SCFT composition profiles of B40 and B40b using the known scattering length densities of the components.^{69,70} These profiles were then fit to a four term Fourier series

$$\rho(zV^{1/3}) = \rho_0 + \sum_{n=1}^3 \Delta\rho_n \cos\left(\frac{2\pi zV^{1/3}}{d/n}\right) \quad (11)$$

where d is the lamellar spacing, ρ_0 is a constant, and $\Delta\rho_n$ are the fitted amplitudes. Further terms beyond third order did not improve fitting noticeably. The results of this exercise for B40 are shown in Figure 10. At all temperatures we obtain a scattering profile that is approximately sinusoidal. For example, at 30 °C, the amplitudes $\Delta\rho_1$, $\Delta\rho_2$, and $\Delta\rho_3$ for the B40 blend at 30 °C were 8.7×10^{-5} , 1.0×10^{-5} , and $-4.2 \times 10^{-6} \text{ nm}^{-2}$, respectively. The solid curve in Figure 10 represents the four term Fourier series fit from which the amplitudes were extracted. Since the scattering intensity at $q = 2\pi n/d$ is proportional to $(\Delta\rho_n)^2$, we expect that the intensity for the second- and third-order peaks will be almost 2 orders of magnitude smaller than the primary peak. This was true at all temperatures up to 90 °C. It is thus no surprise that higher order peaks were not observed in B40 (Figure 5a).

Figure 11 shows the SCFT predictions for the neutron scattering length density profile, ρ , as a function of $zV^{1/3}$ for blend B40b at various temperatures. There are

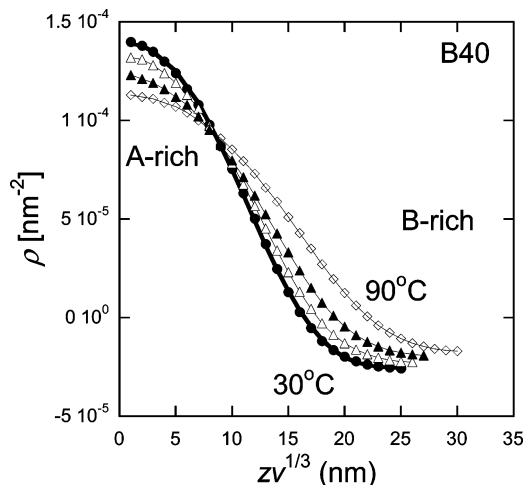


Figure 10. Neutron scattering length density, ρ , vs distance, $zv^{1/3}$, for half a lamellar spacing for blends B40 at 30 (●), 50 (△), 70 (▲), and 90 °C (◇). The solid line through the 30 °C data is a fit using eq 11.

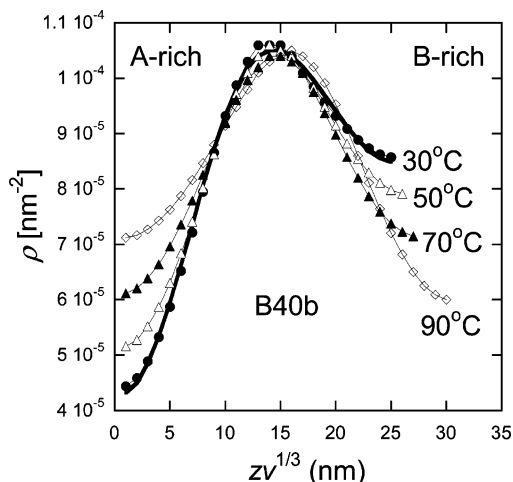


Figure 11. Neutron scattering length density, ρ , vs distance, $zv^{1/3}$, for half a lamellar spacing for blends B40b at 30 (●), 50 (△), 70 (▲), and 90 °C (◇). The solid line through the 30 °C data is a fit using eq 11.

qualitative differences between the scattering length density profiles obtained from B40 and B40b. At all temperatures, the deuterated compound accumulates at the interface between A-rich and B-rich phases. In addition, at 30 °C the neutron scattering length density profile is clearly asymmetric (Figure 11). The scattering length density on the A-rich side of the lamellae is $4.4 \times 10^{-5} \text{ nm}^{-2}$, while that on the B-rich side is $8.6 \times 10^{-5} \text{ nm}^{-2}$ due to the fact that there is much more diblock copolymer in the B-rich region than in the A-rich region. This asymmetry in $\rho(zv^{1/3})$ decreases with increasing temperature. At 70 and 90 °C, the difference in scattering length densities on the A-rich and B-rich sides is less than $1.2 \times 10^{-5} \text{ nm}^{-2}$. We can quantitatively look at these asymmetries by fitting the profile to the four term Fourier series (eq 11). The solid curve in Figure 11 shows the least-squares fit through the 30 °C data, from which we conclude that the Fourier amplitudes $\Delta\rho_1$, $\Delta\rho_2$, and $\Delta\rho_3$ for the B40b blend at 30 °C are 1.9×10^{-5} , 2.0×10^{-5} , and $1.8 \times 10^{-6} \text{ nm}^{-2}$, respectively. Note that $\Delta\rho_1$ and $\Delta\rho_2$ are now comparable in magnitude, while $\Delta\rho_3$ is negligible. We thus expect to observe both primary and secondary peaks in B40b. This is exactly what we have found experimentally (Figure 5b).

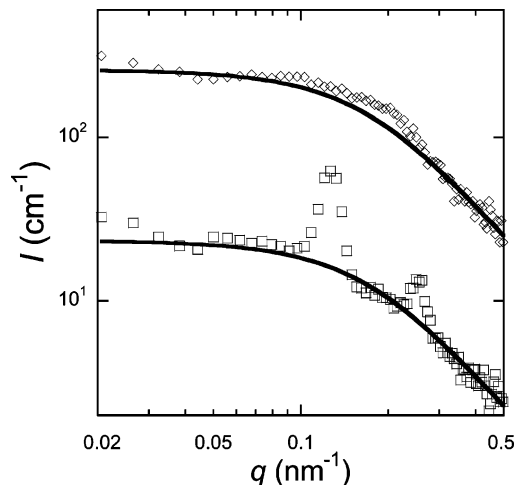


Figure 12. SANS data obtained from B40b at 30 (□) and 70 °C (◇). The data at 70 °C was multiplied by a factor of 10. The Debye function, $I = K(\exp(-R_g^2 q^2) + R_g^2 q^2 - 1)/(R_g^2 q^2)^2$, was fit to the data with the radius of gyration (R_g) and contrast (K) as adjustable parameters (solid lines).

Inspection of the data in Figure 5b suggests that the scattering peaks indicative of the presence of the lamellar phase in B40b lie on a background, which is a monotonic function of q . As is often the case in scattering from polymer systems, the scattering profiles from B40b contain contributions due to the structure of the sample as well as chain connectivity. A reasonable choice for the background function is thus the Debye function (eq 2). In Figure 12, we show both the Debye function (solid line) and the SANS data obtained at 30 and 70 °C for B40b. The value of the radius of gyration (R_g) used in the Debye function, fit at each temperature, was between 87 and 105 nm. The difference between the SANS intensity (I) and the Debye function (I_{Debye}) allows us to focus on changes in the structure of B40b with temperature. We define $\Delta I = I - I_{\text{Debye}}$. In cases where the peak is barely distinguishable from the background, it was difficult to determine the peak location. In these cases (for example at 70 °C) the primary peak position was taken to be the location of the peak for B40 (Figure 5a), and the secondary peak position was taken to be twice the q value of the primary peak. We believe this approach is justified as the primary peak of B40b at 30 °C is at $q = 0.127 \text{ nm}^{-1}$ and the peak of B40 at 30 °C is located at $q = 0.121 \text{ nm}^{-1}$. A plot of ΔI vs q reveals two peaks at 30 °C, as shown in Figure 13: a primary peak at $q = 0.127 \text{ nm}^{-1}$ and a secondary peak at $q = 0.254 \text{ nm}^{-1}$. The SCFT results provide a clear explanation for this observation. The primary peak arises from the scattering contrast between adjacent lamellae while the secondary peak arises from the interfacial accumulation of the block copolymer which has twice the period of the lamellar phase. It is clear from Figure 13 that ΔI at the primary peak position is a sensitive function of temperature, changing from 47 to 3 cm^{-1} when the temperature is changed from 30 to 70 °C. In contrast, ΔI at the secondary peak position is a relatively insensitive function of temperature, changing from 6 to 3 cm^{-1} when the temperature is changed from 30 to 70 °C. This is quantified in Figure 14 where ΔI , normalized by the values of ΔI at 30 °C, for the primary and secondary peaks of B40b are plotted as a function of temperature (filled symbols). Also shown in Figure 14 are the square of the first-order and second-order amplitudes, $(\Delta\rho_1)^2$

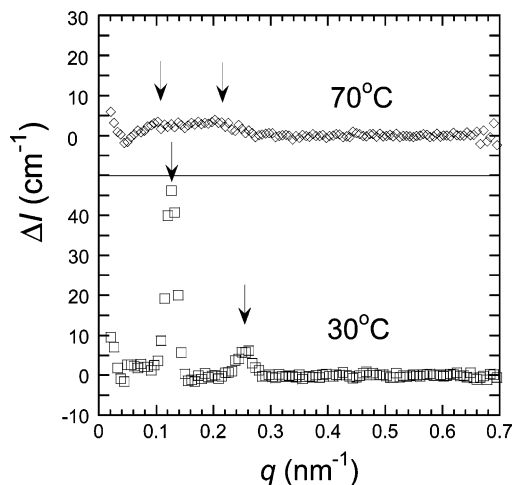


Figure 13. SANS data obtained from B40b at 30 (□) and 70 °C (◇) with the Debye function subtracted from the data. For clarity, each data set has a separate ΔI axis. The arrows point to the locations of the primary and secondary peaks determined through methods described in the text.

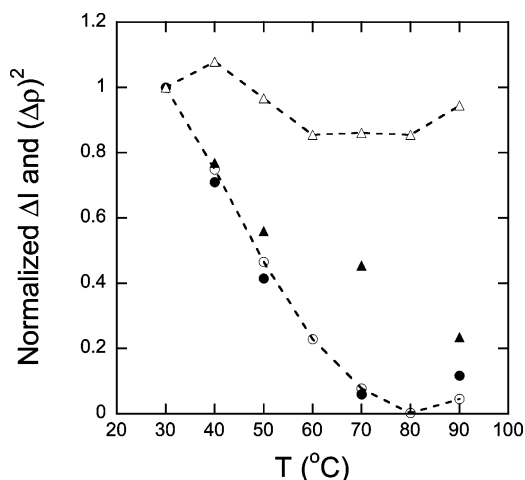


Figure 14. Variation of the primary (circles) and secondary (triangles) SANS peak intensities with temperature for blend B40b obtained by experiment (ΔI , solid symbols) and SCFT ($(\Delta\rho)^2$, open symbols with lines). A quadratic fit was used to determine the value of ΔI . This intensity was then normalized with the value of the intensity at 30 °C. $(\Delta\rho_1)^2$ and $(\Delta\rho_2)^2$ as predicted from the SCFT neutron scattering length density profile were also normalized.

and $(\Delta\rho_2)^2$, obtained from the SCFT calculations (open symbols with lines in Figure 14). We find that $(\Delta\rho_1)^2$ decreases by an order of magnitude in our temperature window while $(\Delta\rho_2)^2$ is insensitive to changes in temperature. This is in qualitative agreement with the SANS data. What is perhaps more remarkable is that the temperature dependencies of ΔI of the primary peak and $(\Delta\rho_1)^2$ are in quantitative agreement (Figure 14). The disappearance of the primary peak in B40b at 70 and 90 °C is thus undoubtedly due to the fact that the scattering contrast between the coexisting microphases diminishes. The SCFT calculations show that the interfacial accumulation of the block copolymer is unaffected by temperature (Figure 11), which implies that $(\Delta\rho_2)^2$ is relatively independent of temperature (Figure 14). This would imply that the ΔI for the secondary peak should not diminish with temperature. In contrast, ΔI of the secondary peak decreases by about a factor of 4 in our temperature range (Figure 14). Another feature of the scattering data incompatible with the SCFT

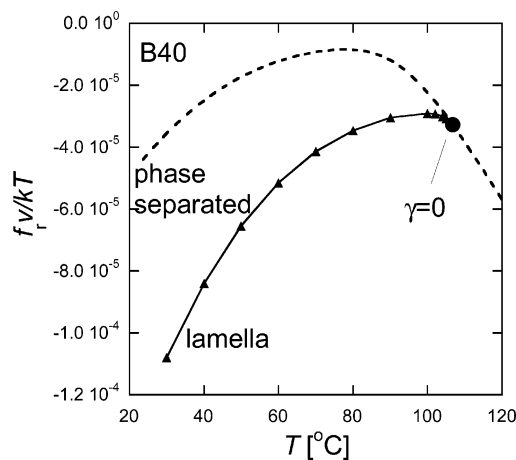


Figure 15. Free energy density as a function of temperature for blend B40. The free energy of a phase-separated system (dashed line) and a lamellar system (solid line) are plotted. The triangles correspond to the results of SCFT calculations. The point on the phase-separated system line at which the interfacial tension vanishes is also plotted (●). The reference free energy density is that of a homogeneous mixed system.

calculations is the relative intensities of the primary and secondary peaks for the B40b blend. Since $(\Delta\rho_1)^2$ and $(\Delta\rho_2)^2$ are comparable, it is expected that the intensities of the peaks should also be similar; however, the primary peak is substantially larger. It is thus clear that all of the features seen in the SANS profiles cannot be quantitatively explained by SCFT. A complete quantitative description of the systems studied here will certainly need to account for fluctuation effects.⁷¹ Despite this limitation, the SCFT calculations provide considerable insight into the origin of our experimental observations.

The analysis described above was repeated for B50b. The results were qualitatively similar to those of B40b and have been omitted for brevity.

The free energy densities of the equilibrium lamellar phases, f_l of B40 and B50, at a given temperature were calculated as described in Appendix B. Triangles in Figure 15 show the temperature dependence of the relative free energy, f_r , obtained for B40, where $f_r = f - f_{\text{homog}}$ and f_{homog} is the free energy of a homogeneous blend from eq 10. The computed lamellar spacings diverge as we approach 107 °C, and thus, the computed free energies of the lamellar phase terminate at this point. Also shown in Figure 15 are the free energies of the phase-separated state (dashed line). The free energy of two coexisting structureless phases is simply the sum of the free energies of the two phases given by eq 10. For a binary polymer blend the phase-equilibrium calculation is solved by the common tangent method. For a ternary polymer blend the problem is essentially the same but the tangent lines are now planes.^{21,72} The average Helmholtz free energy of the phase separated blend is minimized by varying the compositions and volumes of the two phases while restricting the average composition to the known value and keeping the total volume constant. The free energy minimum was found numerically using Newton–Raphson iteration.

Since the free energy of a structureless homogeneous blend is used as the reference, it corresponds to the line $f_r = 0$ in Figure 15. The phase-separated state has a lower free energy than the homogeneous phase at all temperatures (i.e., f_r is negative). At temperatures lower

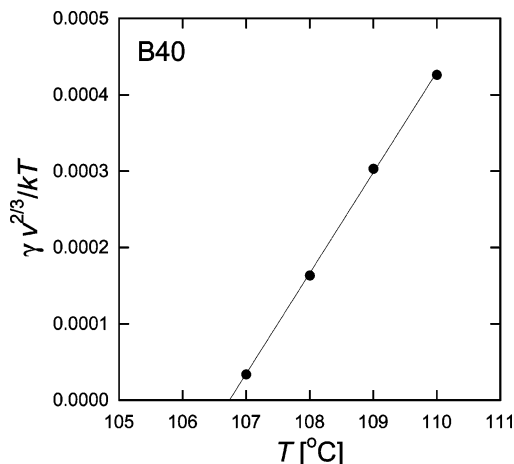


Figure 16. Temperature dependence of the interfacial tension between the two phase-separated phases in blend B40.

than 107 °C, the lamellar state has the lowest free energy of the phases, whereas for temperatures greater than 107 °C the phase-separated blend has the lowest free energy. SCFT thus predicts a lamellar-to-phase separated transition at 107 °C. It is worth noting that at temperatures above this phase transition temperature calculations of the phase-separated compositions predict that the copolymer is predominantly in the A-rich rather than B-rich phase. This accounts for the large increase in low- q SANS intensities seen in the B40b blend at 112 °C (Figure 5b).

Figure 16 shows the temperature dependence of the interfacial tension between the two coexisting macrophases, γ , in blend B40 calculated using SCFT (Appendix B). At high temperatures ($T \geq 107$ °C), where SCFT calculations indicate macrophase separation, the interfacial tension is positive. As the temperature is lowered, the interfacial tension decreases until just below 107 °C it equals zero. At this point the two-phase system will become unstable. The point at which the interfacial tension becomes zero is indicated in Figure 15. The point where the lamellar phase becomes unstable (terminus of the solid curve in Figure 15) and the point where the two-phase system becomes unstable (solid circle in Figure 15) are in excellent agreement for the B40 case. In addition, these theoretical calculations are in excellent agreement with the transition from microphase-separated states to macrophase-separated states of 104 ± 5 °C (Table 5), determined by light scattering.

The SCFT calculations for the B50 blend lead to results that are similar to those obtained from the B40 blend. The free energies of the lamellar and phase-separated states are plotted in Figure 17. In the B50 blend, the lamellar free energy density line in Figure 17 passes through the phase separation free energy density line and continues for a short distance beyond before terminating. The point at which the interfacial tension becomes zero is close to, but not exactly at, this intersection. In addition, the free energies of the phase-separated and lamellar phases near the intersection are similar to that of the homogeneous phase (note that the intersection is near the $f_c = 0$ line). These observations suggest that the transition from lamellae to a macrophase-separated state in B50 is more complex than that in B40. Our best theoretical estimate of the phase separation temperature for the B50 blend is around 110

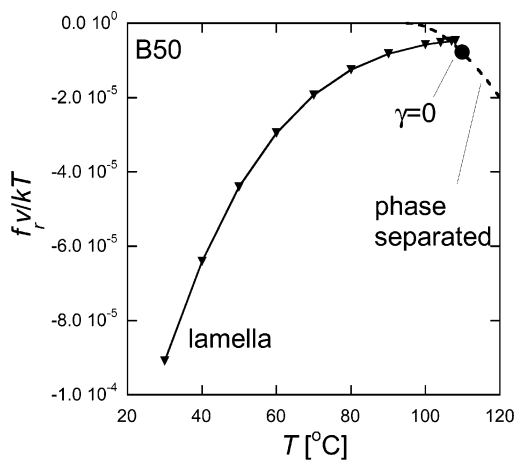


Figure 17. Free energy density as a function of temperature for blend B50. The free energy of a phase-separated system (dashed line) and a lamellar system (solid line) are plotted. The triangles correspond to the results of SCFT calculations. The point on the phase-separated system line at which the interfacial tension vanishes is also plotted (●). The reference free energy density is that of a homogeneous mixed system.

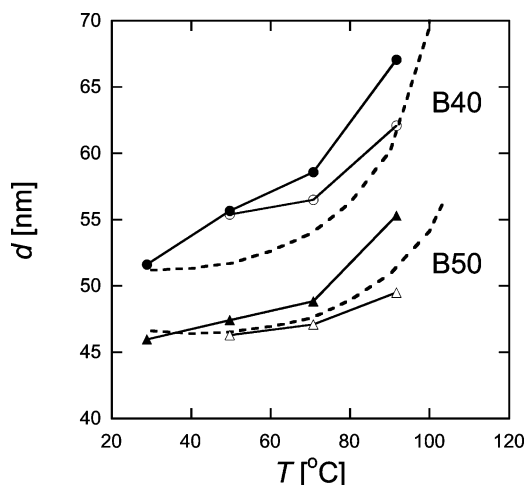


Figure 18. Domain spacings of blends B40 (●, ○), B50 (▲, △) measured using SANS (filled symbols correspond to the domain spacing associated with the location of the maximum intensity peak and empty symbols represent the domain spacing from a Teubner–Strey fit (eq 7)) and predicted by SCFT (dashed lines).

°C, which agrees with the light scattering estimate of 113 ± 5 °C (Table 5).

More demanding experimental checks of the SCFT calculations can be made by comparing the domain spacing seen from the SANS data with those predicted from SCFT. This comparison is presented in Figure 18. For the microemulsion phases we present two measures of the domain spacing, d . One is based on the location of the primary scattering peak ($d = 2\pi/q_{\text{peak}}$), and the other is based on the Teubner–Strey equation (eqs 7 and 9). The SCFT calculations capture the trends of changing temperature and changing volume fraction of diblock copolymer (Figure 18). At 30 °C, we obtained quantitative agreement between theory and experiment in both B40 and B50. Deviations between theory and experiment of 10% (or less) are seen at higher temperatures. Although at temperatures of 70 °C and higher the structures obtained experimentally are microemulsions rather than lamellae, we believe that modeling them as lamellae is a reasonable first approximation.

We expect this to work adequately when the local structure resembles that of lamellae, such as in a bicontinuous microemulsion, but to break down for a droplet microemulsion. The observed deviations between theory and experiment in Figure 18 are reasonable, given the limitations of our one-dimensional SCFT calculations, the uncertainty in the statistical segment lengths ($\sim 5\%$, see Figure 2), and errors introduced by applying parameters from binary blends to a ternary system.

The importance of fluctuations on the thermodynamics of oil/water microemulsions is well-established.⁷³ We were thus surprised by the agreement between our experimental data and our thermodynamic models which do not take fluctuations into account. Whether this is fortuitous for the particular system that we have studied or a simplification that applies more broadly to polymeric A/B/A–C mixtures remains to be seen.

Conclusions

The purpose of this paper is to obtain a fundamental understanding of the factors that govern the thermodynamics of complex multicomponent polymer mixtures wherein both attractive and repulsive interactions are present. The systems chosen for our experiments were mixtures of nearly monodisperse model polyolefins of sPB90, PIB, and a sPB90–sPB63 block copolymer. The Flory–Huggins interaction parameters, χ , between the components and the statistical segment lengths of the components were obtained from small-angle neutron scattering (SANS) experiments from binary homopolymer blends. The χ parameter between PIB and sPB63 is negative over a significant fraction of the accessible temperature window, while the other two χ parameters are positive over the accessible temperature window. Our objective was to examine the possibility of predicting the phase behavior of our multicomponent blends, using only parameters determined from the binary experiments.

Concentration fluctuations in homogeneous multicomponent blends (BH20), studied by SANS, were in quantitative agreement with predictions based on the multicomponent random phase approximation (RPA). SANS and SALS were also used to study the properties of micro- and macrophase-separated multicomponent blends (B40, B40b, B50, and B50b). These blends exhibited ordered lamellae or disordered microemulsion structures at low temperatures and began to phase separate between 90 and 110 °C. Self-consistent field theory (SCFT) was used to model these ternary blends. These calculations enabled quantitative interpretation of the SANS profiles from microphase separated A/B/A–C blends. Comparisons between the SANS data and the SCFT calculations enabled a detailed interpretation of the microphase-separated state of A/B/A–C blends. This includes quantification of the temperature-dependent changes in the composition of the microphases and accumulation of the A–C block copolymer at the interfaces. The phase-separation temperatures calculated for the blends were within the experimental window of 90–110 °C. The lamellar spacings calculated from SCFT were in agreement with the experimentally observed lamellar spacings. All of the comparisons between experiments and the RPA and SCFT predictions were presented without any adjustable parameters.

We have thus shown that the properties of complex multicomponent blends can be predicted using mean-

field theories such as the RPA and SCFT. Mixtures of polyolefins may thus be considered as model systems for studying the molecular origin of interfacial activity. This work sets the stage for establishing rational principles for designing different kinds of surfactants for organizing immiscible polymers. The blends that were the focus of this study were prepared on the basis of intuition and loose analogies between the sPB90–sPB63 block copolymer and balanced nonionic surfactants for oil/water mixtures.^{45–51} We hope to use the models developed here to guide the design of more effective surfactants for controlling the morphology of phase-separated polymer blends. It is perhaps appropriate to note that such predictions have not yet been possible in the case of oil/water/surfactant mixtures.^{74,75}

It is clear that our efforts will benefit from the development of more refined models, wherein the symmetry of the equilibrium structure is calculated rather than assumed.^{76,77} Models that account for departures from mean-field behavior due to the presence of concentration fluctuations may elucidate the nature of the phase transitions that these complex systems are capable of exhibiting.⁷¹ Many models suggest that the Flory–Huggins theory is not an appropriate starting point for describing the thermodynamics of homopolymer blends.^{78,79} While considerable work remains, we believe that this paper represents an important first step toward understanding the origin of interfacial activity and phase behavior in complex polymer systems.

Acknowledgment. Financial support was provided by the National Science Foundation (CTS-0305711). This material is based upon work supported under a National Science Foundation Graduate Research Fellowship. The facilities at NIST are supported in part by the National Science Foundation under Agreement No. DMR-9986442. Support provided by Pamela J. Wright, at ExxonMobil, concerning cationic polymerization is greatly appreciated. The assistance of Margaret Stambaugh, Michael Colin McCarthy, and Julie Chao through their undergraduate research was helpful in obtaining the small-angle light scattering results presented here. The comparison between experiment and the Fourier analysis of the SCFT calculations is due to the extremely valuable criticisms of one of the referees.

Appendix A. Multicomponent Random Phase Approximation

The multicomponent random phase approximation can be used to describe the scattering from a homogeneous blend of two homopolymers (A and B) and a diblock copolymer (A–C).^{32–34} We use the subscripts Ah and Bh to refer to the A and B homopolymers and the subscripts Ab and Cb to refer to the A and C blocks of the copolymer. The subscripts $j, k = (Ah, Ab, Cb)$ simplify the equations. Correlations involving Bh are eliminated by assuming incompressibility. This is done by choosing Bh to be the background component. The coherent scattering profile from an A/B/A–C multicomponent blend is

$$I(q) = \mathbf{B}^T \mathbf{S}(q) \mathbf{B} \quad (\text{A1})$$

where \mathbf{B} is a column vector describing the contrast and $\mathbf{S}(q)$ is the 3×3 structure factor matrix. The elements

of \mathbf{B} are related to the scattering length density of each component j :

$$B_j = \frac{b_j - b_{Bh}}{v} \quad (j = Ah, Ab, Cb) \quad (\text{A2})$$

where v is the reference volume and b_j is the scattering length of a reference volume unit. Because of incompressibility, the correlations with the background component are eliminated as long as the background component is not connected to any of the other components. (In our case the background component is chosen to be the B homopolymer.)

The structure factor matrix is given by

$$\mathbf{S}(q) = [\mathbf{S}^0(q)^{-1} + \mathbf{V}(q)]^{-1} \quad (\text{A3})$$

where $\mathbf{S}^0(q)$ describes the structure factor matrix in the absence of interactions and $\mathbf{V}(q)$ describes the interactions between all of the components. The components of $\mathbf{S}^0(q)$ and $\mathbf{V}(q)$ are given as follows:

$$S_{jj}^0(q) = N_j \phi_j v P_j(q) \quad (j = Ah, Ab, Cb) \quad (\text{A4})$$

$$S_{AbCb}^0(q) = S_{CbAb}^0(q) = (N_{Ab} \phi_{Ab} N_{Cb} \phi_{Cb})^{1/2} v F_{Ab}(q) F_{Cb}(q) \quad (\text{A5})$$

$$S_{AbAh}^0(q) = S_{CbAh}^0(q) = S_{AhAb}^0(q) = S_{AhCb}^0(q) = 0 \quad (\text{A6})$$

$$V_{jj}(q) = \frac{1}{v} \left(\frac{1}{N_{Bh} \phi_{Bh} P_{Bh}(q)} - 2\chi_{jBh} \right) \quad (j = Ah, Ab, Cb) \quad (\text{A7})$$

$$V_{jk}(q) = \frac{1}{v} \left(\frac{1}{N_{Bh} \phi_{Bh} P_{Bh}(q)} - \chi_{jBh} - \chi_{kBh} + \chi_{jk} \right) \quad (j \neq k) \quad (\text{A8})$$

$$F_j(q) = \frac{1 - \exp(-x_m)}{x_m} \quad (\text{A9})$$

where ϕ_j is the volume fraction of each component j in the blend and $P_j(q)$ and x_m are defined in the main text. The following parameters are based upon a reference volume of $v = 100 \text{ \AA}^3$: N_j (the number of reference volume units of each component j), l_j (the statistical segment length of each component j), and the Flory–Huggins interaction parameters χ_{jk} .

Appendix B. Self-Consistent Field Theory

Self-consistent field theory is used to describe periodic structures where the volume fractions of the components are periodic functions of position, $\phi_{i,m}(z)$. The notation $\phi_{i,m}(z)$ represents the volume fraction of units of type m from species of type i , where $m = (A, B, C)$, $i = (Ah, Bh, ACb)$, and z is a Cartesian one-dimensional coordinate made dimensionless using $v^{1/3}$. In this appendix the term “unit” will refer to a reference volume unit of polymer. In a blend of polymers of different types of monomers, the field experienced by a unit of type m , w_m , is

$$w_m(z) = \xi(z) + E_m(z) \quad (\text{B1})$$

$$E_m(z) = \sum_n \chi_{mn} \phi_n(z) \quad (\text{B2})$$

where $\xi(z)$ is a field, independent of monomer type, that enforces the incompressibility constraint, $E_m(z)$ is the field representing the interactions of units of type m with their surroundings, χ_{mn} is the Flory–Huggins interaction parameter between units of type m and n , and $\phi_n(z)$ is the volume fraction of units of type n at position z . The function $\xi(z)$ is expressed in terms of the excess energy field, $\Delta w(z)$

$$\xi(z) = \Delta w(z) - \sum_i \frac{\phi_i(z)}{N_i} - \sum_{m,n} \chi_{mn} \phi_m(z) \phi_n(z) \quad (\text{B3})$$

$$\Delta w(z) = \zeta \left(\sum_i \phi_i(z) - 1 \right) \quad (\text{B4})$$

where ζ is the inverse of the isothermal compressibility of the mixture (ζ is constant). In our calculations, ζ is chosen to be a sufficiently large value to ensure that the blend is essentially incompressible (i.e., that the sum of the volume fractions approaches one).

The parameter s defines units along the chain of a species and runs from 0 to N_i for species of type i . If we constrain a unit, s , on a chain (of species i) to be held at position z in space, the partition function of the section of the chain from 0 to s is described by

$$\frac{\partial q_i(z,s)}{\partial s} = \sum_m \sigma_{i,m}(s) \left[\frac{\tilde{l}_m^2}{6} \frac{d^2}{dz^2} q_i(z,s) - w_m q_i(z,s) \right], \quad q_i(z,0) = 1 \quad (\text{B5})$$

Here $\tilde{l}_m = l_m v^{1/3}$ is the dimensionless statistical segment length of chains of monomer m , and $\sigma_{i,m}(s)$ is 1 if at position s in a species of type i there is a m unit and 0 otherwise. The partition function of the entire chain, $Q_i(z,s)$, can then be written as the product of the partition functions of the complementary chain sections.

$$Q_i(z,s) = q_i(z,s) q_i^*(z,s) \quad (\text{B6})$$

where q_i^* is similar to q_i but is the partition function of the section of the chain from s to N_i . In both cases, position s is anchored at z . The governing equation for q_i^* is similar to eq B5 but with a negative sign in front of the right-hand side and with the boundary condition $q_i^*(z, N_i) = 1$.

The volume fraction of units of type m from species of type i at position z is then

$$\phi_{i,m}(z) = C_i \int_{s=0}^{N_i} ds \sigma_{i,m}(s) Q_i(z,s) \quad (\text{B7})$$

where C_i is a normalization constant. Since the total volume fraction of species of type i in the system, ϕ_i , is known, C_i can be obtained from

$$C_i = \frac{\phi_i M}{\int_0^{N_i} \int_0^M dz ds Q_i(z,s)} \quad (\text{B8})$$

where the integration over z is performed from $z = 0$ to M (the left and right boundaries of the box). The volume fraction of units of type m at position z can simply be found by summing the contribution over the polymer types

$$\phi_m(z) = \sum_i \phi_{i,m}(z) \quad (\text{B9})$$

We start with an initial guess for $\phi_m(z)$ and calculate the fields using eqs B1–B4. From these fields the partition functions $Q_i(z,s)$ are calculated with eqs B5 and B6. A finite difference approximation of eq B5 is

$$q_i(z,s) = \sum_m \sigma_{i,m} \left[\left(1 - \frac{\tilde{\gamma}_m^2 \Delta s}{3 \Delta z^2} \right) q_i(z,s - \Delta s) + \frac{\tilde{\gamma}_m^2 \Delta s}{6 \Delta z^2} q_i(z - \Delta z, s - \Delta s) + \frac{\tilde{\gamma}_m^2 \Delta s}{6 \Delta z^2} q_i(z + \Delta z, s - \Delta s) \right] e^{-w_m(z)\Delta s} \quad (\text{B10})$$

where Δs and Δz are the size of the discrete steps taken. All calculations reported use $\Delta s = 3.71$ and $\Delta z = 2.15$.⁸⁰ It is necessary that N_i is a multiple of Δs , so N_i is rounded to the nearest multiple, and compensating corrections are made to the statistical segment lengths, $\tilde{\gamma}_m$, and fields, $w_m(z)$, to minimize discontinuous changes in the free energy density with temperature. The volume fractions are found with eqs B7–B9. Fields are calculated from the new volume fraction profiles again using eqs B1–B4 and are combined with the previous fields for numerical stability

$$E_A(z)_{\text{new}} = \lambda_1 E_A(z)_{\text{calculated}} + (1 - \lambda_1) E_A(z)_{\text{old}} \quad (\text{B11})$$

$$\xi(z)_{\text{new}} = \lambda_2 \xi(z)_{\text{calculated}} + (1 - \lambda_2) \xi(z)_{\text{old}} \quad (\text{B12})$$

where λ_1 is typically 0.1 and λ_2 is typically 0.001. λ_1 and λ_2 are chosen to be as large as is possible without the iterations becoming unstable.

The new fields are then used to generate a new concentration profile, and the process is iterated until convergence. Convergence is judged to have occurred when the change in the free energy density at each iteration step is well below the required level of accuracy. The error due to incomplete convergence is in all cases smaller than the size of the data points in the plots.

When a self-consistent solution is found, the free energy density of the polymers in the external fields, f^{ext} , can be calculated from the partition function in the usual way.

$$\frac{f^{\text{ext}}_V}{kT} = -\frac{\ln Q}{V} = -\sum_i \frac{\phi_i}{N_i} (\ln Q_i - \ln Q_i^{\text{ref}}) \quad (\text{B13})$$

$$Q_i = \frac{V}{N_i M} \int_0^M dz \int_0^{N_i} ds Q_i(z,s) \quad (\text{B14})$$

$$\ln Q_i^{\text{ref}} = \ln(\phi_i V) + N_i \sum_m \frac{\phi_{i,m}}{\phi_i} w_{i,m}^{\text{ref}} \quad (\text{B15})$$

where Q is the partition function for the entire system, V is the volume of the entire system, Q_i is the partition function of a species of type i , Q_i^{ref} is the partition function of a species of type i in its reference state, M is the box width, and $w_{i,m}^{\text{ref}}$ is the field that a unit of type m experiences in the reference state of species i . The

reference state we will use is that of each species forming a pure structureless phase. The free energy density that we wish to calculate is not the free energy density of the polymers in the external field but the free energy density of the system of interacting polymers, f . Since the entropy of the two systems will be the same, it is only necessary to make an adjustment to the energy.³⁷ In eq B16 the energy of the polymer interactions is added, and the energy of the external field is deducted.

$$\begin{aligned} \frac{f_V}{kT} &= \frac{f^{\text{ext}}_V}{kT} + \\ &\left[\frac{1}{M} \int_0^M dz \left(\sum_{m,n} \chi_{mn} \phi_m(z) \phi_n(z) - \sum_i \frac{1}{\phi_i} \sum_{m,n} \chi_{mn} \phi_{i,m} \phi_{i,n} \right) \right] - \\ &\left[\frac{1}{M} \int_0^M dz \sum_m \phi_m(z) w_m(z) - \sum_{i,m} \phi_{i,m} w_{i,m}^{\text{ref}} \right] \\ &= \sum_i \frac{\phi_i}{N_i} \left(\ln \left(\frac{\phi_i V}{Q_i} \right) + 1 - \frac{N_i}{\phi_i} \sum_{m,n} \chi_{mn} \phi_{i,m} \phi_{i,n} \right) - \\ &\frac{1}{M} \int_0^M dz \Delta w(z) \quad (\text{B16}) \end{aligned}$$

We used the above procedure to compute f , the free energy density of lamellar phases.

We also calculate the interfacial tension between the two phases of a phase separated blend using self-consistent field theory. In this case, a large box ($M \gg$ radius of gyration of the biggest chain) is modeled so that at the edges of the box the volume fractions reach their bulk levels and are not influenced by the presence of the interface. In a phase-separated blend there is very little interface; thus, the polymer adsorbed at the interface does not contribute to the average volume fractions. In the simulation box, there is relatively much more interface, so adsorbed polymer does contribute to the average volume fraction. This means that we cannot use eq B8 to calculate the normalization constants for the volume fractions. Instead of basing the normalization constants on the average volume fractions, we base them on the volume fractions at the edge of the box, where they reach the bulk levels. We use ϕ_i for the average volume fractions in the simulation box and θ_i for the average volume fractions in the blend. The volume fractions at the edges of the box, $\phi_i^{\text{A-rich}}$ and $\phi_i^{\text{B-rich}}$, are related to the volume fractions of the blend, θ_i , by

$$\alpha \phi_i^{\text{A-rich}} + (1 - \alpha) \phi_i^{\text{B-rich}} = \theta_i \quad (\text{B17})$$

$$\phi_i^{\text{A-rich}} = C_i \int_{s=0}^{N_i} ds Q_i(0,s) \quad (\text{B18})$$

$$\phi_i^{\text{B-rich}} = C_i \int_{s=0}^{N_i} ds Q_i(M,s) \quad (\text{B19})$$

where α is the fraction of the blend in the A-rich phase and $(1 - \alpha)$ is the fraction of the blend in the B-rich phase, and $z = M$ and $z = 0$ are the two edges of the box. Since this problem is underspecified by one variable (the position of the interface in the box), we also specify the average volume fraction of one of the components, ϕ_{Ah} , and solve for C_{Ah} using eq B8. We then solve for α and determine all of the other normalization constants C_i .

Once the self-consistent solution has been established, the interfacial tension, γ , can be calculated using^{81,82}

$$\frac{v^{2/3}\gamma}{kT} = -\int_0^M dz \Delta w(z) \quad (\text{B20})$$

Δw is equal to 0 in the bulk because of the way we defined our normalization constants. As long as the integration is performed over the entire interface, the limits of integration in eq B20 are not important.

In modeling the phase behavior of A/B/A-C blends, we do not attempt to obtain an accurate description of the microemulsion phase, which requires the incorporation of fluctuation corrections. These theories are outside the scope of the present analysis. The SCFT calculations in this paper are thus restricted to one linear dimension in position space.

To calculate the free energy of a lamellar phase formed at a given temperature and overall blend composition, we choose a box size of about half the expected lamellar spacing and impose reflective boundary conditions. Reflective boundary conditions are imposed by replacing the $q(z-\Delta z, s-\Delta s)$ term in eq B10 with a $q(z, s-\Delta s)$ term at the left boundary and replacing the $q(z+\Delta z, s-\Delta s)$ term in eq B10 with a $q(z, s-\Delta s)$ term at the right boundary. Since it is not important that the composition of the initial guess matches the actual composition, we make the initial guess that one-half of the box is pure homopolymer A and the second half is pure homopolymer B. The SCFT calculations then allow us to compute the equilibrium composition profiles, $\phi_{i,m}(z)$, and the free energy density, f .

References and Notes

- Bates, F. S.; Maurer, W.; Lodge, T. P.; Schulz, M. F.; Matsen, M. W.; Almdal, K.; Mortensen, K. *Phys. Rev. Lett.* **1995**, *75*, 4429.
- Hillmyer, M. A.; Maurer, W. W.; Lodge, T. P.; Bates, F. S.; Almdal, K. *J. Phys. Chem. B* **1999**, *103*, 4814.
- Bates, F. S.; Maurer, W. W.; Lipic, P. M.; Hillmyer, M. A.; Almdal, K.; Mortensen, K.; Fredrickson, G. H.; Lodge, T. P. *Phys. Rev. Lett.* **1997**, *79*, 849.
- Washburn, N. R.; Lodge, T. P.; Bates, F. S. *J. Phys. Chem. B* **2000**, *104*, 6987.
- Morkved, T. L.; Chapman, B. R.; Bates, F. S.; Lodge, T. P.; Stepanek, P.; Almdal, K. *Faraday Discuss.* **1999**, *112*, 335.
- Cohen, R. E.; Ramos, A. R. *Macromolecules* **1979**, *12*, 131.
- Datta, S.; Lohse, D. J. *Polymeric Compatibilizers*; Hanser: Cincinnati, OH, 1996.
- Hudson, S. D.; Jamieson, A. M. In *Polymer Blends*; Paul, C. B., Ed.; Wiley: New York, 2000; Vol. 1.
- Jeon, H. S.; Lee, J. H.; Balsara, N. P. *Phys. Rev. Lett.* **1997**, *79*, 3274.
- Jeon, H. S.; Lee, J. H.; Balsara, N. P. *Macromolecules* **1998**, *31*, 3328.
- Jeon, H. S.; Lee, J. H.; Balsara, N. P.; Newstein, M. C. *Macromolecules* **1998**, *31*, 3340.
- Lyu, S.; Jones, T. D.; Bates, F. S.; Macosko, C. W. *Macromolecules* **2002**, *35*, 7845.
- Tan, N. C. B.; Tai, S. K.; Briber, R. M. *Polymer* **1996**, *37*, 3509.
- Jackson, C. L.; Sung, L.; Han, C. C. *Polym. Eng. Sci.* **1997**, *37*, 1449.
- Sung, L.; Hess, D. B.; Jackson, C. L.; Han, C. C. *J. Polym. Res. (Taiwan)* **1996**, *3*, 139.
- Koizumi, S.; Hasegawa, H.; Hashimoto, T. *Macromolecules* **1994**, *27*, 7893.
- Kielhorn, L.; Muthukumar, M. *J. Chem. Phys.* **1997**, *107*, 5588.
- Balsara, N. P.; Jonnalagadda, S. V.; Lin, C. C.; Han, C. C.; Krishnamoorti, R. *J. Chem. Phys.* **1993**, *99*, 10011.
- Leibler, L. *Makromol. Chem., Macromol. Symp.* **1988**, *16*, 1.
- Leibler, L. *Physica A* **1991**, *172*, 258.
- Broseta, D.; Fredrickson, G. H. *J. Chem. Phys.* **1990**, *93*, 2927.
- Mathur, D.; Hariharan, R.; Neuman, E. B. *Polymer* **1999**, *40*, 6077.
- Wang, Z. G.; Safran, S. A. *J. Phys. (Paris)* **1990**, *51*, 185.
- Janert, P. K.; Schick, M. *Macromolecules* **1997**, *30*, 3916.
- Janert, P. K.; Schick, M. *Macromolecules* **1997**, *30*, 137.
- Muller, M.; Schick, M. *J. Chem. Phys.* **1996**, *105*, 8885.
- Maric, M.; Macosko, C. W. *J. Polym. Sci., Polym. Phys.* **2002**, *40*, 346.
- Schnell, R.; Stamm, M.; Rauch, F. *Macromol. Chem. Phys.* **1999**, *200*, 1806.
- Zhao, H. Y.; Huang, B. T. *J. Polym. Sci., Polym. Phys.* **1998**, *36*, 85.
- Flory, P. J. *J. Chem. Phys.* **1941**, *9*, 660.
- Huggins, M. *J. Chem. Phys.* **1941**, *9*, 440.
- de Gennes, P. G. In *Scaling Concepts in Polymer Physics*; Cornell University Press: Ithaca, NY, 1979; Chapter 9.
- Akcasu, A. Z.; Tombakoglu, M. *Macromolecules* **1990**, *23*, 607.
- Benoit, H.; Benmouna, M.; Wu, W. L. *Macromolecules* **1990**, *23*, 1511.
- Helfand, E. *J. Chem. Phys.* **1975**, *62*, 999.
- Evers, O. A.; Scheutjens, J. M. H. M.; Fleer, G. J. *Macromolecules* **1990**, *23*, 5221.
- Matsen, M. W. *J. Phys.: Condens. Matter* **2002**, *14*, R21.
- Typically the thermodynamic effects of the statistical segments lengths are small.
- Shull, K. R.; Mayes, A. M.; Russell, T. P. *Macromolecules* **1993**, *26*, 3929.
- Lodge, T. P.; Hamersky, M. W.; Hanley, K. J.; Huang, C. I. *Macromolecules* **1997**, *30*, 6139.
- Matsen, M. W. *J. Chem. Phys.* **1999**, *110*, 4658.
- Lee, J. H.; Ruegg, M. L.; Balsara, N. P.; Zhu, Y. Q.; Gido, S. P.; Krishnamoorti, R.; Kim, M. H. *Macromolecules* **2003**, *36*, 6537.
- Lee, J. H.; Balsara, N. P.; Chakraborty, A. K.; Krishnamoorti, R.; Hammouda, B. *Macromolecules* **2002**, *35*, 7748.
- Lee, J. H.; Balsara, N. P.; Krishnamoorti, R.; Jeon, H. S.; Hammouda, B. *Macromolecules* **2001**, *34*, 6557.
- Kahlweit, M.; Strey, R. *Angew. Chem., Int. Ed. Engl.* **1985**, *24*, 654.
- Kahlweit, M.; Strey, R.; Firman, P.; Haase, D. *Langmuir* **1985**, *1*, 281.
- Kahlweit, M.; Strey, R.; Haase, D.; Firman, P. *Langmuir* **1988**, *4*, 785.
- Strey, R. *Colloid Polym. Sci.* **1994**, *272*, 1005.
- Chen, S. H.; Choi, S. *Supramol. Sci.* **1998**, *5*, 197.
- Magid, L.; Butler, P.; Payne, K.; Strey, R. *J. Appl. Crystallogr.* **1988**, *21*, 832.
- Teubner, M.; Strey, R. *J. Chem. Phys.* **1987**, *87*, 3195.
- Kline, S. *SANS Data Reduction Tutorial*, NIST Center for Neutron Research, 2001.
- Balsara, N. P.; Lohse, D. J.; Graessley, W. W.; Krishnamoorti, R. *J. Chem. Phys.* **1994**, *100*, 3905.
- Lee, J. H. PhD Thesis, University of California, Berkeley, CA, 2002; p 151.
- Fredrickson, G. H.; Milner, S. T.; Leibler, L. *Macromolecules* **1992**, *25*, 6341.
- Krishnamoorti, R. PhD Thesis, Princeton University, Princeton, NJ, 1994; p 504.
- The thermal expansion coefficients used in the determination of the temperature dependence of reference unit volumes are as follows: $7.0 \times 10^{-4} \text{ K}^{-1}$ for sPB90, $7.2 \times 10^{-4} \text{ K}^{-1}$ for sPB63, and $5.7 \times 10^{-4} \text{ K}^{-1}$ for PIB.
- Fetters, L. J.; Lohse, D. J.; Colby, R. H. In *Physical Properties of Polymers Handbook*; AIP Press: New York, 1996; Chapter 24.
- Krishnamoorti, R.; Graessley, W. W.; Fetters, L. J.; Garner, R. T.; Lohse, D. J. *Macromolecules* **1995**, *28*, 1252.
- Graessley, W. W.; Krishnamoorti, R.; Balsara, N. P.; Fetters, L. J.; Lohse, D. J.; Schulz, D. N.; Sissano, J. A. *Macromolecules* **1994**, *27*, 2574.
- Fitting the χ vs T data to a line of the form $\chi = A + B/T$ gives the following parameters: $A = 0.00627$ and $B = -0.518 \text{ K}$ for the A/B blend, $A = -0.00372$ and $B = 2.98 \text{ K}$ for the A/C blend, and $A = 0.0186$ and $B = -7.22$ for the B/C blend.
- Graessley, W. W.; Krishnamoorti, R.; Balsara, N. P.; Fetters, L. J.; Lohse, D. J.; Schulz, D. N.; Sissano, J. A. *Macromolecules* **1993**, *26*, 1137.
- Graessley, W. W.; Krishnamoorti, R.; Balsara, N. P.; Butera, R. J.; Fetters, L. J.; Lohse, D. J.; Schulz, D. N.; Sissano, J. A. *Macromolecules* **1994**, *27*, 3896.
- Wignall, G. D.; Bates, F. S. *Makromol. Chem., Macromol. Symp.* **1988**, *15*, 105.

- (65) Jeon, H. S.; Lee, J. H.; Balsara, N. P. *Macromolecules* **1998**, *31*, 3328.
- (66) This quadratic background was used because the Debye function was unsuccessful at fitting the high- q data.
- (67) The Debye function was fit to each data set to determine the background scattering. This was then subtracted from the data. The peak position was determined through fitting a quadratic curve of the form $y = ax^2 + bx + c$ to the data (minus the Debye background), where a , b , and c are fitting parameters. The peak position, $q_{\text{peak}} = -b/(2a)$.
- (68) Balsara, N. P.; Fetters, L. J.; Hadjichristidis, N.; Lohse, D. J.; Han, C. C.; Graessley, W. W.; Krishnamoorti, R. *Macromolecules* **1992**, *25*, 6137.
- (69) Neutron scattering length densities of selected polymers used in this study: hPB90(35) = $-3.09 \times 10^{-5} \text{ nm}^{-2}$, dPB90(35) = $2.16 \times 10^{-4} \text{ nm}^{-2}$, PIB(45) = $-3.26 \times 10^{-5} \text{ nm}^{-2}$, hPBPB-(38-41) block A = $3.09 \times 10^{-5} \text{ nm}^{-2}$, and hPBPB(38-41) block C = $3.09 \times 10^{-4} \text{ nm}^{-2}$, dPBPB(38-41) block A = $2.38 \times 10^{-4} \text{ nm}^{-2}$, and dPBPB(38-41) block C = $2.78 \times 10^{-4} \text{ nm}^{-2}$. The neutron scattering lengths for the blocks of the diblock copolymer were determined using methods outlined in ref 70.
- (70) Ruegg, M. L.; Newstein, M. C.; Balsara, N. P.; Reynolds, B. J. *Macromolecules* **2004**, *37*, 1960.
- (71) Ganesan, V.; Fredrickson, G. H. *Europhys. Lett.* **2001**, *55*, 814.
- (72) Leibler, L. *Makromol. Chem., Rapid Commun.* **1981**, *2*, 393.
- (73) Talmon, Y.; Prager, S. *Nature (London)* **1977**, *267*, 333.
- (74) Schick, M.; Shih, W. *Phys. Rev. Lett.* **1987**, *59*, 1205.
- (75) Gompper, G.; Schick, M. *Phys. Rev. Lett.* **1989**, *62*, 1647.
- (76) Drolet, F.; Fredrickson, G. H. *Phys. Rev. Lett.* **1999**, *83*, 4317.
- (77) Bohbot-Raviv, Y.; Wang, Z. G. *Phys. Rev. Lett.* **2000**, *85*, 3428.
- (78) Ruzette, A. G.; Mayes, A. M. *Macromolecules* **2001**, *34*, 1894.
- (79) Dudowicz, J.; Freed, K. F.; Douglas, J. F. *Phys. Rev. Lett.* **2002**, *88*, 095503.
- (80) Δs and Δz were chosen as a compromise between speed and accuracy. The smaller the values, the better an approximation eq B10 is to eq B5, but the calculation becomes slower. Δs and Δz are chosen to keep $l_m \Delta s / \Delta z^2$ equal to approximately 1.0 so that eq B10 is stable.
- (81) Genzer, J.; Faldi, A.; Composto, R. J. *J. Chem. Phys.* **1996**, *105*, 10134.
- (82) Matsen, M. W.; Gardiner, J. M. *J. Chem. Phys.* **2001**, *115*, 2794.

MA049779D